

# 1 **Patterns and drivers of dimethylsulfide concentration in the northeast** 2 **Subarctic Pacific across multiple spatial and temporal scales**

3 Alysia E. Herr<sup>1</sup>, Ronald P. Kiene<sup>2</sup>, John W. H. Dacey<sup>3</sup>, Philippe D. Tortell<sup>1,4</sup>

4 <sup>1</sup>Department of Earth, Ocean and Atmospheric Sciences, University of British Columbia, Vancouver, BC, V6T 1Z4, Canada

5 <sup>2</sup>Department of Marine Sciences, University of South Alabama, Mobile, AL, 36688, USA

6 <sup>3</sup>Woods Hole Oceanographic Institute, Woods Hole, MA, 02543, USA

7 <sup>4</sup>Department of Botany, University of British Columbia, Vancouver, BC, V6T 1Z4, Canada

8 *Correspondence to:* Alysia E. Herr (aherr@eoas.ubc.ca)

## 9 **Abstract.**

10

11 The northeast subarctic Pacific (NESAP) is a globally important source of the climate-active gas dimethylsulfide (DMS), yet  
12 the processes driving DMS variability across this region are poorly understood. Here we examine the spatial distribution of  
13 DMS at various spatial scales in contrasting oceanographic regimes of the NESAP. We present new high spatial resolution  
14 measurements of DMS across hydrographic frontal zones along the British Columbia continental shelf, together with key  
15 environmental variables and biological rate measurements. We combine these new data with existing observations to produce  
16 a revised summertime DMS climatology for the NESAP, yielding a broader context for our sub-mesoscale process studies.  
17 Our results demonstrate sharp DMS concentration gradients across hydrographic frontal zones, and suggest the presence of  
18 two distinct DMS cycling regimes in the NESAP, corresponding to microphytoplankton-dominated waters along the  
19 continental shelf, and nanoplankton-dominated waters in the cross-shelf transitional zone. DMS concentrations across the  
20 continental shelf transition (range <1–10 nM, mean 3.9 nM) exhibited positive correlations to salinity ( $r=0.80$ ), sea surface  
21 height anomaly (SSHA;  $r=0.51$ ) and the relative abundance of prymnesiophyte and dinoflagellates ( $r=0.89$ ). In contrast, DMS  
22 concentrations in near shore coastal transects (range <1–24 nM, mean 6.1 nM) showed a negative correlation with salinity ( $r=-$   
23  $0.69$ ,  $r=-0.78$ ) and SSHA ( $r=-0.81$ ,  $r=-0.75$ ), and a positive correlation to relative diatom abundance ( $r=0.88$ ,  $r=0.86$ ). These  
24 results highlight the importance of bloom-driven DMS production in continental shelf waters of this region, and the role of  
25 prymnesiophytes and dinoflagellates in DMS cycling further offshore. In all areas, the rate of DMS consumption appeared to  
26 be an important control on observed concentration gradients, with higher DMS consumption rate constants associated with  
27 lower DMS concentrations. We compiled a dataset of all available summertime DMS observations for the NESAP (including  
28 previously unpublished results) to examine the performance of several existing algorithms to predict regional DMS  
29 concentrations. None of these existing algorithms was able to accurately reproduce observed DMS distributions across the  
30 NESAP, although performance was improved by the use of regionally tuned-coefficients. Based on our compiled observations,

1 we derived an average summertime distribution map for DMS concentrations and sea–air fluxes across the NESAP, estimating  
2 a mean regional flux of 0.30 Tg of DMS-derived sulfur to the atmosphere during the summer season.

### 3 **1 Introduction**

4 Spurred by a proposed role in climate regulation as a source of cloud-condensation nuclei and back-scattering aerosols, the  
5 biogenic trace gas dimethylsulfide (DMS) and related organic sulfur compounds dimethylsulfoniopropionate (DMSP) and  
6 dimethyl sulfoxide (DMSO) have been studied for more than four decades (Lovelock et al. 1972; Charlson et al. 1987). This  
7 body of research has revealed complex sulfur biogeochemical cycling in the oceans, and important physiological and  
8 ecological roles for these molecules (Simó 2004; Stefels et al. 2007). DMSP and DMS have been shown to play an essential  
9 function in marine microbial systems as sources of carbon and sulfur (Kiene et al. 2000; Reisch et al. 2011). These molecules  
10 also act as olfactory foraging cues for numerous species of birds, fish, marine invertebrates and mammals (Seymour et al.  
11 2010; Johnson et al. 2016), thereby driving interactions both within and beyond the marine microbial food web. The ecological,  
12 chemical and climatological significance of DMS and related compounds has stimulated significant effort to understand the  
13 surface ocean distribution of these molecules and the underlying factors driving their variability.

14

15 The Pacific Marine Environmental Laboratory (PMEL) has compiled a database of over 47,000 discrete DMS measurements.  
16 Lana et al. (2011, hereafter L11) utilized these data to construct a global climatology of surface ocean DMS concentrations  
17 and sea–air fluxes, providing broad-scale understanding of oceanic distribution patterns. The global mean DMS concentration  
18 is estimated to be approximately 2 nM, but the climatology reveals several regional ‘hot spots’ of elevated DMS accumulation,  
19 including polynya waters of the Southern Ocean, and the northeast Subarctic Pacific (NESAP). In these regions, surface ocean  
20 DMS concentrations 5–10-fold higher than the mean oceanic value are commonly observed (Kiene et al., 2007; Lana et al.  
21 2011, Jarníková and Tortell 2016). Although large-scale global patterns derived from the climatology are likely robust, a fuller  
22 understanding of spatial and temporal patterns of regional DMS variability is constrained by the relatively poor spatial and  
23 temporal coverage of existing measurements.

24

25 The NESAP, defined here as the region bounded by 44.5° N and 61° N latitude and 180° W and 120° W, exhibits consistently  
26 high summertime DMS concentrations in both open ocean and coastal regions, with maxima of ~20 nM observed during the  
27 late summer season (Wong et al. 2005; Asher et al. 2011, 2017; Steiner et al. 2012). This oceanic region is also characterized  
28 by strong spatial heterogeneity of environmental characteristics. High-productivity coastal upwelling regions transition to iron-  
29 limited high nutrient low chlorophyll (HNLC) waters offshore (Boyd and Harrison 1999; Boyd et al. 2004). Seasonally varying  
30 surface currents, fresh water inputs, coastal upwelling and recurrent formation of westward-propagating mesoscale eddies  
31 result in semi-permanent and transient hydrographic frontal zones, impacting regional marine biodiversity and productivity

1 (Crawford et al. 2005; Whitney et al. 2005; Ribalet et al. 2010). This spatial heterogeneity makes it challenging to quantify  
2 DMS distributions from discrete ship-based sampling, and complicates region-wide generalizations of DMS dynamics.  
3  
4 Recent work has highlighted differences in the distribution of DMS and related compounds across distinct domains of the  
5 NESAP, particularly in offshore and coastal regions (Wong et al. 2005; Asher et al. 2011, 2017; Steiner et al. 2012). The  
6 HNLC offshore region was identified by L11 as an area of high DMS concentrations and sea–air fluxes. Results from in situ  
7 observations (Wong et al. 2005; Lavoie et al. 2006; Merzouk et al. 2006; Asher et al. 2011) and numerical models (Steiner  
8 et al. 2012) suggest that elevated DMS concentrations in these open ocean waters are driven by the presence of high DMS/P  
9 producing phytoplankton taxa, such as prymnesiophytes and dinoflagellates, and the effects of mixed layer stratification and  
10 Fe-limitation, which may act to increase DMS/P production as a means to offset oxidative stress (Sunda et al. 2002, Kinsey et  
11 al. 2016). A low particulate organic carbon to sulfur ratio in the HNLC regime further influences bacterial DMSP metabolism,  
12 resulting in increased DMS-yield from DMSP metabolism (Merzouk et al. 2006; Royer et al. 2010). In the physically dynamic  
13 coastal waters of the NESAP, high DMS concentrations likely result, in part, from seasonal coastal upwelling, which drives  
14 high phytoplankton biomass accumulation. Recent work (Asher et al. 2017) has demonstrated an enhancement of DMS  
15 accumulation following upwelling events in the coastal NESAP, consistent with previously observed high DMS/P  
16 concentrations in other upwelling regions (Hatton et al. 1998; Zindler et al. 2012; Wu et al. 2017). Increased DMS  
17 concentrations in the post-upwelling bloom phase may result from nitrogen limitation, increased grazing pressure (which  
18 releases DMSP into the dissolved pool; Simó et al. 2018), oxidative stress associated with shoaling mixed layers, and a  
19 phytoplankton community shift towards high DMSP-producing species (Nemcek et al. 2008; Franklin et al. 2009). Despite  
20 these advances in understanding DMS dynamics in the NESAP, many aspects of DMS cycling in this region remain poorly  
21 documented, including the factors influencing interannual variability (Steiner et al., 2012; Galí et al., 2018), the interplay  
22 between iron concentration and phytoplankton community shifts (Lavoie et al. 2006; Roayer et al. 2010), and the relative  
23 importance of phytoplanktonic DMSP lyases and micrograzers (Steiner et al. 2012).  
24  
25 New advances in sensor technology over the past decade have begun to significantly expand DMS data coverage in a number  
26 of ocean regions. These fine scale measurements reveal novel features and highlight the apparent influence of oceanographic  
27 frontal zones in driving fine-scale DMS distribution patterns (Holligan et al. 1987; Locarnini et al. 1998; Belviso et al. 2003;  
28 Tortell 2005a; Nemcek et al. 2008; Royer et al. 2015; Jarníková et al. 2018). In previous work (Asher et al. 2017), we have  
29 documented sharp transitions in DMS concentrations across salinity frontal zones in nearshore NESAP waters. This earlier  
30 work did not include corresponding measurements of DMS/P turnover rates, limiting mechanistic interpretation of the observed  
31 spatial patterns. To our knowledge, there has been no systematic evaluation of the processes driving fine-scale DMS variability  
32 across frontal zones. Such a study requires high resolution concentration measurements together with assessments of  
33 biological productivity and DMS/P turnover rates.  
34

1 In this article, we present a new data set of DMS/P concentrations across coastal and open ocean waters of the Subarctic  
2 Pacific, from the northern Gulf of Alaska to the Oregon coast. Using a suite of measurements collected during two summer  
3 cruises (2016–2017), we document regional-scale features, and characterize sub-mesoscale DMS structure across  
4 hydrographic frontal zones in on-shelf and transition regions. Using real-time ship-board measurements, we were able to  
5 select contrasting sites across frontal zones for more extensive sampling and analysis, allowing us to probe underlying rate  
6 processes in adjacent areas with distinct DMS/P concentrations and surface water hydrography. We combined our new data  
7 set with existing observations from our own group and from the existing PMEL database to produce a new summertime DMS  
8 climatology for the NESAP. This updated climatology enables us to better constrain the summertime distribution of DMS in  
9 the NESAP, identifying persistent ‘hot spots’, and exploring correlations between DMS concentration and other biotic and  
10 abiotic variables. We also use our compiled data set to evaluate various empirical algorithms predicting DMS concentrations  
11 and sea–air fluxes across the NESAP. Our results yield new insights into the spatial patterns and potential drivers of  
12 summertime NESAP DMS distribution across various spatial scales in a globally important oceanic region.

## 13 **2 Methods**

### 14 **2.1 Data overview**

15 In this study, we combined new data from two recent oceanographic expeditions with existing observations derived from  
16 several decades of compiled DMS measurements in the NESAP. Ancillary measurements of various environmental and  
17 biological variables were obtained from a number of sources (ship-based measurements, remote sensing and blended data  
18 products) to help interpret DMS distribution patterns. The various data sets are described below.

### 19 **2.2 New high-resolution data sets**

#### 20 **2.2.1 Underway ship-board measurements**

21 Field sampling was conducted on board the University–National Oceanographic Laboratory System (UNOLS) vessel *Oceanus*  
22 during July of 2016 and August of 2017 (O16, O17, respectively). Our cruise tracks included offshore, coastal and transitional  
23 waters throughout the Gulf of Alaska (Fig. 1). We define the coastal regime as those waters with bottom depths shallower  
24 than 2000 m, following Asher et al. (2011). We utilized real-time DMS measurements (see below) and NASA satellite ocean  
25 colour imagery (AquaMODIS) to guide our cruise track, enabling us to identify areas with high concentrations of DMS and  
26 strong spatial gradients in surface water phytoplankton biomass and hydrography (sea surface temperature and salinity).  
27 During O16 we also conducted detailed surveys of three hydrographic frontal zones that exhibited sharp DMS concentration  
28 gradients. One of these surveys (T1; Fig. 1) was located in the coastal-open ocean transition near Dixon Entrance north of  
29 Haida Gwaii (formerly the Queen Charlotte Islands), while the other two transects were located along the British Columbia  
30 continental shelf (T2: Hecate Strait and T3: La Perouse Bank; Fig. 1). After an initial survey to examine frontal structure,

1 stations were selected for depth-resolved sampling to cover the gradients present across the frontal zone. The O17 cruise  
2 covered a similar area as O16. Although we did not perform detailed transect surveys on this second cruise, we did sample  
3 waters near T1–T3.

4  
5 High resolution surface water DMS measurements were conducted using membrane inlet mass spectrometry (MIMS)  
6 following published methods (Tortell 2005b; Nemcek et al. 2008). The MIMS system, sampling from the ship's underway  
7 seawater flow through system (~5 m intake depth), allows for high-frequency measurements (2–3 times per minute), yielding  
8 a spatial resolution of ~150–200 m at normal ship speeds of 8–10 kts. During these cruises, DMS concentrations were also  
9 measured in discrete water samples collected at 5 m depth using a purge-and-trap system connected to a gas chromatograph  
10 equipped with a flame-photometric detector (FPD-GC) (Kiene and Service 1991). These discrete measurements were used to  
11 assess the accuracy of MIMS-based measurements. We found good agreement between methods, with a mean absolute error  
12 of 0.90 nM, root mean square error of 1.4 nM, and coefficient of determination of  $r^2=0.89$  between the two instruments across  
13 the full range of measured concentrations (Fig. 3).

14  
15 High resolution DMS measurements were paired with rate measurements and ancillary underway data to examine potential  
16 drivers of spatial variation. A ship-board thermosalinograph was used to measure sea surface temperature (SST) and salinity  
17 at high spatial resolution (SBE 45 and SBE 38 for salinity and temperature, respectively). Chlorophyll-*a* (chl-*a*) concentration  
18 was measured using a WET labs ACS absorbance/attenuation meter, based on the absorption line height at 676 nm (Bricaud  
19 et al. 1995; Roesler and Barnard 2013; Burt et al. 2018). These chl-*a* concentrations were further used to derive an estimate  
20 of phytoplankton assemblage size structure and taxonomic distributions, based on the empirical algorithm of Hirata et al.  
21 (2011). Phytoplankton size-class estimates derived from this algorithm agreed well ( $r^2 > 0.75$ ) with discrete HPLC-derived  
22 estimates (methods described below; Zeng et al. 2018). MIMS was also used to determine the ratio of oxygen and argon  
23 concentrations relative to atmospheric saturation. The resulting biological oxygen saturation term,  $\Delta O_2/Ar$ , can be used to  
24 calculate net community productivity (NCP) from the air–sea gas exchange of  $O_2$  (Kaiser et al. 2005). We used the calculation  
25 approach of Reuer et al. (2007) to compute NCP from our  $\Delta O_2/Ar$  measurements. We note that some of these estimates,  
26 particularly in regions of active upwelling, are likely negatively biased by the entrainment of  $O_2$  under-saturated water into the  
27 mixed layer. While this effect can be accounted for using  $N_2O$  measurements (Izett et al. 2018), we do not have these data  
28 available for our cruises. Our derived NCP estimates thus likely represent under-estimates, and we have removed all negative  
29 NCP values. Nonetheless, the general spatial patterns we observed in NCP are likely to be robust.

### 30 **2.2.2 Station-based measurements**

31 We measured a suite of variables at selected sampling stations along the cruise track. All water for ancillary measurements  
32 was taken from 5 m depth, collected using Niskin bottles. A Seabird CTD probe (Seabird 911plus) was deployed at each

1 station to obtain depth profiles of hydrographic features over the upper 200 m of the water column. A density difference  
2 criterion of  $0.05 \text{ kg m}^{-3}$  was used to calculate mixed layer depths.

3

4 DMS loss and DMSP consumption rates were measured using the radio-labeled  $^{35}\text{S}$  methods outlined by Kiene and Linn (2000)  
5 with some modifications to minimize the release of DMSPd during incubations. Briefly,  $^{35}\text{S}$ -labeled DMSPd or DMS were  
6 added to samples at non-perturbing concentrations ( $<1\%$  of ambient levels). Samples were incubated in the dark at surface  
7 water temperatures for  $<1 \text{ h}$  ( $^{35}\text{S}$ -DMSP) or  $<7 \text{ h}$  ( $^{35}\text{S}$ -DMS). The rate constant for DMSPd turnover was determined by  
8 measuring the disappearance of  $^{35}\text{S}$ -DMSP from the dissolved ( $< 0.2 \mu\text{m}$ ) pool. The rate constants for DMS loss were  
9 determined by measuring the accumulation of dissolved, non-volatile  $^{35}\text{S}$  transformation products derived from the volatile  
10  $^{35}\text{S}$ -DMS tracer. Consumption rates ( $\text{nmol L}^{-1} \text{ d}^{-1}$ ) were calculated by multiplying in situ DMS or DMSPd concentrations by  
11 the measured rate constant ( $k_{\text{DMS}}$  or  $k_{\text{DMSPd}}$  respectively).

12

13 Primary productivity was measured using 24 h  $^{14}\text{C}$  uptake incubations, following the method outlined by Schuback et al.  
14 (2015). Incubation bottles were held in a deck-board incubator plumbed with continuously flowing seawater to achieve in situ  
15 temperature. The light intensity was adjusted to  $\sim 30\%$  surface irradiance enriched in blue light using neutral density screening  
16 in combination with blue photographic film (LEE filters: #209 and CT blue maximum transmission at approximately 460 nm).  
17 Light levels in the tank were measured with a ULM-500 light meter equipped with a  $4\pi$ -sensor (Walz). Bacterial production  
18 was measured using the tritiated leucine method (Smith and Azam 1992) and converted to carbon units (Simon and Azam  
19 1989; Ducklow et al. 2000). Station samples were also analysed for total and dissolved DMSP (DMSPt and DMSPd) with a  
20 GC-FPD discrete method using the previously described NaOH cleavage and small-volume gravity drip filtration method  
21 (Dacey and Blough 1987; Kiene and Slezak 2006). DMSPP was calculated by subtracting DMSPd from DMSPt (Zindler et  
22 al. 2012, Levine et al. 2016).

23

24 We obtained discrete estimates of phytoplankton assemblage composition using diagnostic pigment analysis (DPA) of  
25 photosynthetic pigments measured using HPLC. For these measurements, 1 L samples were collected on GF/F filters (nominal  
26 pore size  $\sim 0.7 \mu\text{m}$ ), flash frozen in liquid nitrogen and stored frozen until analysis at the NASA Goddard Space Flight Center  
27 Ocean Ecology Laboratory (Van Heukelem and Thomas 2001). The DPA method was originally developed by Vidussi et al.  
28 (2001), and subsequently refined (Uitz et al. 2006; Hirata et al. 2008; Brewin et al. 2010) to more accurately capture  
29 phytoplankton type and size class. The estimation formulas used here are those of Hirata et al. (2011), with coefficients tuned  
30 specifically for the NESAP by Zeng et al. (2018). Percent contribution to phytoplankton assemblage was assessed for three  
31 size classes (micro, nano, and pico).

## 1 **2.3 Compilation of published data**

2 To provide a broader regional spatial context for our observations, we combined discrete DMS measurements from the PMEL  
3 data archive with high spatial resolution DMS measurements made using MIMS since the early 2000s. Table 1 provides dates  
4 and spatial domains of the cruises, along with relevant literature citations. Note that some of the DMS data included in this  
5 compilation have not been previously published. All of our compiled MIMS data have been made available on the PMEL  
6 database (<https://saga.pmel.noaa.gov/dms/>).

### 7 **2.3.1 MIMS data sets**

8 MIMS-based observations included in this study are derived from 11 cruises conducted between 2004 and 2017, primarily  
9 aboard the Canadian Coast Guard Ship *John P. Tully* as part of ongoing time-series monitoring programs conducted by the  
10 Department of Fisheries and Oceans Canada (DFO). Only summertime data (defined here as June, July and August; JJA)  
11 falling within the NESAP region (44.5°–61° N, 180°–120° W) were included in this compilation. Although DMS  
12 concentrations and phytoplankton biomass often remains high through September (Galí et al., 2018; Lana et al., 2011; Steiner  
13 et al., 2012), there are fewer DMS data available for this month. Measurements were binned to a temporal sampling resolution  
14 of 1 minute. All DMS data points are paired with shipboard sea surface salinity and SST. The cruises VIJ04, VIJ10, WCAC10,  
15 LPA11, O16 and O17 also include paired NCP estimates obtained from MIMS measurements, using the  $\Delta\text{O}_2/\text{Ar}$ -based method  
16 described above.

### 17 **2.3.2 PMEL data extraction**

18 We accessed the PMEL data base (<http://saga.pmel.noaa.gov/dms/>) on 6 December, 2017 to extract observations from June,  
19 July and August in the NESAP region defined above. Our selection criteria yielded 3236 data points between 1984 and 2003.  
20 These observations were relatively evenly distributed between the three months, but were biased spatially, with a  
21 preponderance of data derived from on-shelf waters off the coast of Alaska (see Fig. 8b). As with MIMS data, the majority of  
22 data points in the PMEL data base included paired sea surface salinity and SST measurements (94.6% and 99.8%, respectively).

## 23 **2.4 Ancillary measurements**

24 Ancillary oceanographic data were used to contextualize DMS spatial distributions, examine potential correlations to  
25 environmental variables and evaluate the performance of several empirical algorithms predicting DMS concentrations. In  
26 many cases, ancillary variables of interest (e.g. chl-*a*) were not reported in conjunction with DMS data, and we thus utilized a  
27 number of remote sensing data products, as described below. Remotely-sensed parameters were linearly interpolated to the  
28 spatial resolution of ship-based DMS observations.

29

1 AquaMODIS satellite data were used to obtain information on photosynthetically available radiation (PAR; Frouin et al. 2003),  
2 chl-*a* (OCI algorithm; O'Reilly et al. 1998; Hu et al. 2012), calcite (Gordon et al. 2001; Balch et al. 2005) and diffuse  
3 attenuation coefficients (Werdell and Bailey 2005). For these data products, we extracted level 3 gridded data from  
4 <http://oceancolor.gsfc.nasa.gov/cgi/l3> at 9 km resolution. Monthly means for chl-*a*, calcite and  $k_d$  were utilized to maximize  
5 spatial coverage by minimizing data gaps caused by cloudiness, whereas 8 day average PAR data were used. AquaMODIS  
6 chlorophyll and sea surface temperature (SST) data were also used to estimate sea surface nitrate (SSN) using a North Pacific-  
7 specific algorithm (Goes et al. 2000). Aqua MODIS data are only available starting in July of 2002, whereas most of the  
8 PMEL data set in this region is from sampling prior to 2003. For earlier observations (going back to 1997), we used chl-*a* data  
9 from the SeaWiFS satellite. Satellite chl-*a*, calcite and  $k_d$  data were unavailable for data prior to 1997 (<1% of DMS data).

10

11 We obtained information on sea-surface height anomalies (SSHA) using gridded data sets (5 day,  $0.17^\circ \times 0.17^\circ$  resolution)  
12 obtained from [ftp://podaac-ftp.jpl.nasa.gov/allData/merged\\_alt/L4/cdr\\_grid\\_interim](ftp://podaac-ftp.jpl.nasa.gov/allData/merged_alt/L4/cdr_grid_interim). This level 4 satellite product is derived  
13 from various sensors, and data are not available before 1992. Mixed layer depths at a monthly,  $1^\circ$  resolution were obtained  
14 from the China Second Institute of Oceanography (CSIO) [ftp://data.argo.org.cn/pub/ARGO/BOA\\_Argo/](ftp://data.argo.org.cn/pub/ARGO/BOA_Argo/). These data are based  
15 on gridded Argo float data interpolated using the Barnes method, and are available for the years 2004–present (Li et al. 2017).  
16 Due to limitations in Argo operational depths, data are largely absent from waters shallower than 2000 m (136 out of 249  $1^\circ \times$   
17  $1^\circ$  bins).

18

19 We calculated sea–air DMS fluxes from DMS concentration data and surface wind-speeds using the gas transfer  
20 parameterization of Sweeney et al. (2007) and the Schmidt number formulation of Saltzman et al. (1993). Wind speed data  
21 for flux calculations were obtained from the NCEP/NCAR reanalysis dataset  
22 (<https://www.esrl.noaa.gov/psd/data/gridded/data.ncep.reanalysis.pressure.html>) at a  $2.5^\circ$  daily resolution. These calculations  
23 were performed prior to data binning (described below), such that temporally-resolved sea–air flux was calculated for all  
24 ~150,000 DMS data points. Following previous studies, we assume negligible atmospheric DMS concentrations for our  
25 calculations, leading to a potential (though likely small) overestimate of the sea–air flux. For purposes of comparison to fluxes,  
26 we calculated DMS column burden along transects by multiplying DMS concentration and average mixed layer depth.

## 27 **2.5 Data binning and province assignment**

28 High resolution, underway measurements may introduce sampling biases due the large number of data points collected. For  
29 example, a ship holding station will increase spatial data density at a particular location, and the large number of observations  
30 can exert a disproportionate influence on derived mean values. To address this, all measurements in the data set were assigned  
31 to  $1^\circ$  spatial bins, in which all observations for a given year were averaged. All observations within the JJA months for a given  
32 year were averaged, rather than deriving separate monthly climatologies. The resulting yearly data grids were then averaged



1 to create long-term gridded means. This technique effectively assigns equal weight to each year of measurements in a given  
2 grid cell. Both DMS and paired ancillary parameters were binned using this method.

3  
4 Following the approach of L11, data grid cells were assigned to Longhurst Biogeochemical Provinces to examine patterns  
5 across different regimes within the greater NESAP (Longhurst 2007). Three primary provinces fall within the domain of our  
6 study region: California Upwelling Coastal Province (CCAL), Alaska Downwelling Coastal Province (ALSK), and Pacific  
7 Subarctic Gyres Province – East (PSAE) (Fig. 8). The CCAL province as defined by Longhurst extends south to 16.5° N.  
8 Hereafter, all references to the CCAL refer to the portion of this province above 44.5° N latitude. Province boundary  
9 designations were obtained from [www.marineregions.com](http://www.marineregions.com) (accessed October 2017), and the MATLAB native `inpolygon.m`  
10 function was used to assign grid cells to individual provinces. Any grid cell either inside or on the edge of boundaries was  
11 assigned to a particular province. As such, some data cells (37 out of 249 total) are assigned to multiple provinces. Average  
12 summer DMS concentrations and flux measurements were computed for each province. For comparison to L11, we  
13 recalculated the average summertime DMS concentration and flux in the three study provinces using only the PMEL data  
14 utilized by L11. The PMEL data were first binned using the year-weighted method described above.

## 15 **2.6 Statistical analysis and empirical algorithms**

16 We used our compiled data set to examine broad-scale relationships between DMS and other oceanographic variables. For  
17 this analysis, data were log-transformed to overcome non-normal distributions, and the strength of pair-wise relationships was  
18 assessed by computing Pearson's correlation coefficients. Correlations were applied to 1° x 1° binned data both within  
19 individual provinces and across the entire NESAP.

20  
21 We also used several existing empirical algorithms to reconstruct DMS fields at a 1° x 1° resolution from various environmental  
22 predictor variables, comparing the accuracy of the resultant products against our binned DMS observations. The algorithms  
23 tested in this study include those of Simó and Dachs (2002), Vallina and Simó (2007), Watanabe et al. (2007), and Galí et al.  
24 (2018) (hereafter, SD02, VS07, W07, and G18, respectively). Both SD02 and VS07 used global data bases to develop their  
25 algorithms. SD02 relates DMS to chl-*a*:MLD, with chl-*a* values > 15 µg L<sup>-1</sup> removed prior to analysis. VS07 relates DMS  
26 concentration to solar radiative dose (SRD). This term, as defined by the authors, is based on light extinction coefficients ( $k_d$ ),  
27 sea surface irradiance ( $I_0$ ), and mixed layer depth. Due to the large areal extent of the study area, we used AquaMODIS derived  
28 PAR in lieu of the station-based  $I_0$  measurements used by the authors. Similarly, strong variation in  $k_d$  in coastal vs. open  
29 ocean waters is expected. We thus modified the author's approach and used satellite derived  $k_d$  (based on a chlorophyll-  
30 dependent algorithm; Werdell and Bailey 2005) rather than a fixed coefficient. W07 uses data specific to the North Pacific  
31 and relates DMS to SST, SSN and latitude. The two-step G18 algorithm utilizes a previously developed DMSpt predictive  
32 algorithm based on chl-*a* and MLD (Galí et al. 2015), in conjunction with PAR measurements. In order to test this algorithm,  
33 we utilized the satellite-derived PAR, MLD and chl-*a*, described above. We further modify the author's approach by testing

1 performance on our  $1^\circ \times 1^\circ$  binned data, rather than data binned at a  $5^\circ \times 5^\circ$ , in order to maximize the number of observations.  
2 Recognizing the utility of re-parameterizing proposed algorithms for specific areas, we tested algorithms using both published  
3 linear coefficients, and coefficients derived specifically for the NESAP using a least-squares approach to determine best fit to  
4 our data set. The coefficients used to test the original G18 were those regionally tuned by the authors for latitudes above  $45^\circ$   
5 N.

### 6 **3 Results**

7 We begin by presenting an overview of our new DMS measurements and ancillary data from the 2016–2017 summer cruises,  
8 highlighting DMS distributions and the presence of distinct surface water properties across different parts of our transect. We  
9 then provide a detailed description of DMS dynamics across several hydrographic frontal zones, discussing the potential role  
10 of various processes in driving these gradients. Finally, we present an updated summertime climatology for this region,  
11 compiling our new measurements with existing DMS observations from across the NESAP to examine large-scale patterns in  
12 DMS distributions, and correlations with other oceanographic variables. The potential role of these variables in driving DMS  
13 distributions in the NESAP, and the need for additional process studies is addressed in the discussion.

#### 14 **3.1 Oceanographic conditions in the NESAP during summer 2016–2017**

15 Our 2016 and 2017 cruises surveyed oceanographic regimes from offshore HNLC regions to productive coastal upwelling  
16 zones. As indicated by AquaMODIS satellite imagery, chl-*a* concentrations exhibited strong gradients across the oceanic-  
17 coastal transition in both 2016 and 2017 (Fig. 1). Coastal waters showed elevated chl-*a*, with maximum values of  $50 \mu\text{g L}^{-1}$   
18 and  $18 \mu\text{g L}^{-1}$  in 2016 and 2017, respectively. In both years, highest chl-*a* values were observed in waters with shallow mixed-  
19 layer depths ( $<10$  m) along the La Perouse Bank (Fig. 1). In the off-shelf regions, chl-*a* concentrations appeared uniformly  
20 low in 2016, although significant cloud cover limited the availability of satellite imagery. By comparison, we observed  
21 generally higher chl-*a* concentrations in offshore waters in 2017. Most notably, our cruise track passed through an apparent  
22 coccolithophore bloom in the northern Gulf of Alaska, where a large calcite signal ( $\sim 2 \text{ mmol PIC m}^{-3}$ ) was detected in  
23 AquaMODIS imagery. Patterns in NCP were generally similar to those of chl-*a*, with elevated production in coastal waters  
24 (Fig. 2c). In both years, we observed NCP on La Perouse Bank exceeding  $100 \text{ mmol O}_2 \text{ m}^{-2} \text{ d}^{-1}$  (Fig. 2c, inset).

25  
26 Coastal regions exhibited generally fresher surface waters and shallower mixed layer depths, except for several regions of  
27 enhanced vertical mixing associated with upwelling. This coastal upwelling signature was apparent in elevated salinity and  
28 decreased temperature of surface waters, and also through the presence of negative sea surface height anomalies (Fig. 1c,d).  
29 Small-scale regional heterogeneity in coastal regions was apparent in both years, with salinity and temperature exhibiting sharp  
30 gradients over the continental shelf, associated with riverine input and complex mixing processes. By comparison, oceanic  
31 surface waters showed less spatial heterogeneity, and were generally more saline, with deeper mixed layers (Fig. 2b). The

1 sea-surface height anomaly field indicated the presence of several Sitka and Haida eddies in both years (Fig. 1c,d), enhancing  
2 mesoscale variability through the transport of coastal water offshore.  
3  
4 Using the approach of Hirata et al. (2011) and Zeng et al. (2018), we derived high resolution estimates of phytoplankton  
5 assemblage composition from our underway chl-*a* measurements. This approach revealed a predominance of phytoplankton  
6 in the micro- size class (>20  $\mu\text{m}$ ) in coastal waters (Fig. 2d), with an average of 50 % of chl-*a* attributable to  
7 microphytoplankton. In contrast, off-shelf waters showed greater diversity in phytoplankton composition. In these waters,  
8 microphytoplankton accounted for ~25 % of total chl-*a*, while the pico- and nano- size classes accounted for ~30 % and ~40  
9 %, respectively (Fig. 2e,f).

## 10 **3.2 DMS distributions**

11 Across our study region, surface water DMS concentrations ranged from <1–24 nM in 2016 and <1–18 nM in 2017 (Fig. 2a,  
12 Fig. 3). We observed a number of localized DMS ‘hot spots’ in regions of elevated chl-*a* and NCP. In both years, these  
13 localized high DMS regions were particularly evident in the vicinity of the highly productive La Perouse Bank (Fig. 2a, inset).  
14 We also observed several areas where strong DMS gradients co-occurred with salinity fronts. These areas include the T1–T3  
15 transects survey in O16, detailed below. Despite associations between DMS concentration and several variables in some  
16 localized regions, we only observed weak correlations between DMS and other measured variables across the full cruise tracks.  
17 During O16, DMS concentrations were most strongly correlated to NCP, with a Pearson’s coefficient of  $r=0.42$  ( $p<0.001$ ).  
18 This relationship was substantially weaker in O17 ( $r=0.29$ ,  $p<0.001$ ).

## 19 **3.3 Detailed surveys of DMS across hydrographic frontal zones**

20 During the O16 cruise, we sampled along three repeated transects to map DMS distributions near hydrographic frontal zones.  
21 All three transects showed significant gradients in salinity, chl-*a* and DMS/P concentrations, as well as in the metabolic activity  
22 of phytoplankton and bacteria (Fig. 4, 6–7). While DMS concentrations appeared to co-vary with salinity and chl-*a* across  
23 these frontal zones, the strength and direction of these relationships were not consistent across the three transects. We discuss  
24 each transect in detail below.

### 25 **3.3.1 Transect 1**

26 T1 was located west of Dixon Entrance (Fig. 1) in waters influenced by the Alaska Current and coastal water masses. Offshore  
27 waters along this transect were more saline and colder than those on the shelf. The area exhibited DMS concentrations up to  
28 10 nM in off-shelf, saline waters (Fig. 4). Particulate and dissolved DMSP ranged from ~60–125 nM and ~1.8–4.7 nM,  
29 respectively, and showed no significant correlation to DMS (Fig. 4d). At the shelf break (approx. 134.4° W, indicated on Fig.  
30 4 by dotted line), we measured a sharp drop in salinity and corresponding decrease in DMS concentrations, with concentrations

1 remaining below ~3 nM over the most coastal parts of the transect. Across the entire T1 transect, DMS concentrations  
2 displayed a striking fine-scale coherence to salinity ( $r=0.80$ ,  $p<0.001$ ; Fig. 4a,b). A significant positive correlation was also  
3 observed with SSHA ( $r=0.51$ ,  $p<0.001$ ), indicating a potential influence of westward-propagating Haida eddies. Fig. 5 shows  
4 a line plot of SSHA measurements from the approximate time of T1 sampling, overlaid by DMS concentrations. The coherence  
5 between DMS concentrations and mesoscale oceanographic features can be seen in this figure despite differences in the spatial  
6 resolution of the two data sets.

7  
8 The lower salinity coastal waters along T1 were characterized by elevated chl-*a* concentrations (Fig. 4c), resulting in a negative  
9 correlation between DMS concentrations and chlorophyll ( $r=-0.47$ ,  $p<0.001$ ). Figure 4c shows the estimated percent  
10 abundance of diatoms and combined dinoflagellates and prymnesiophytes as derived from HPLC-based DPA-analysis. The  
11 remaining phytoplankton assemblage consisted largely of picoeukaryotes (13 – 36 %). Although HPLC samples are not  
12 available for all of the coastal waters we sampled, results obtained from the empirical algorithm of Hirata et al. (2011) using  
13 underway absorption data suggest a shift in phytoplankton assemblage composition from smaller size classes in offshore waters  
14 to a microphytoplankton-dominated community in on-shelf waters. DMS exhibited relatively weak, though statistically  
15 significant ( $p<0.001$ ) positive correlations with the algorithm-derived relative abundance of nano- and picophytoplankton size-  
16 classes ( $r=0.55$  and  $r=0.38$ , respectively), and a negative correlation with the relative abundance of microphytoplankton ( $r=-$   
17  $0.53$ ). In support of this result, discrete HPLC measurements revealed a strong positive relationship between DMS  
18 concentration and the combined relative abundance of prymnesiophytes and dinoflagellates ( $r=0.89$ ,  $p=0.001$ ), and a negative  
19 correlation to diatom abundance ( $r=-0.70$ ,  $p=0.036$ ). We also observed a strong positive correlation between DMS and  
20 DMSPp:chl-*a* ( $r=0.80$ ,  $p=0.003$ ) suggesting higher cellular DMSP concentrations in phytoplankton assemblages in the off-  
21 shelf regions of this transect. Overall, results from this transect demonstrate a transition from high DMS concentrations in the  
22 lower productivity, nanophytoplankton dominated offshore waters, to low DMS concentrations in higher productivity, diatom-  
23 dominated nearshore region.

24  
25 Average rate constants ( $d^{-1}$ ) for biological consumption of DMS and DMSPd appeared qualitatively higher in the on-shelf  
26 region (although insufficient sampling does not allow for reliable statistical testing), suggesting faster removal of DMS/P from  
27 coastal surface waters with lower DMS concentrations. For DMS and DMSPd respectively, loss constants averaged  $1.15 \pm$   
28  $0.3 d^{-1}$  and  $88.2 \pm 13.9 d^{-1}$  onshore, as compared to  $0.66 \pm 0.045 d^{-1}$  and  $39.6 \pm 1.45 d^{-1}$  in offshore stations (Fig. 4e). Net  
29 primary productivity and bacterial productivity also showed a qualitative trend towards higher average values in the low DMS  
30 coastal waters, but these differences were not statistically significant. Although biological loss of DMS constitutes only one  
31 of several loss terms, the patterns observed here suggest that enhanced microbial activity and relatively higher DMS/P  
32 consumption rate constants played a role in maintaining lower concentrations of these compounds in nearshore waters.

33

1 We calculated the mixed layer DMS burden by multiplying concentration and average mixed layer depth (13 m). Biological  
2 DMS loss integrated over the mixed layer averaged  $22 \mu\text{mol m}^{-2} \text{d}^{-1}$ , sufficient for daily removal of 47 % of the DMS burden.  
3 By comparison, derived sea–air flux estimates across the transect exhibited a mean value of  $13 \mu\text{mol DMS m}^{-2} \text{d}^{-1}$ , accounting  
4 for ~ 25 % of the mixed layer DMS burden daily. Due to a relatively homogenous wind field over the area of our sampling  
5 transect, the sea–air fluxes were tightly correlated to DMS concentrations, such that the lower DMS concentrations in nearshore  
6 regions cannot be explained by greater rates of ventilation to the atmosphere.

### 7 **3.3.2 Transect 2**

8 The second sampling transect, T2, was located in the coastal waters of Hecate Strait situated on the continental shelf (Fig. 1).  
9 Sea surface temperatures along this transect exhibited low variability (standard deviation  $\sim 0.5^\circ \text{C}$ ), with the coldest waters  
10 located mid-transect in areas of highest chl-*a*. Mixed layer depths ranged from 10–15 m, and DMS concentrations ranged  
11 from  $< 0.5 \text{ nM}$  to nearly  $20 \text{ nM}$  (Fig. 6). DMSPd concentrations exhibited only minor variations over the transect ( $2.5\text{--}2.8$   
12  $\text{nM}$ ), while DMSPp concentrations showed greater variability ( $61\text{--}144 \text{ nM}$ ). Neither  
13 DMSPd or DMSPp were correlated to DMS concentrations. HPLC measurements suggested that diatoms dominated across  
14 the entire transect, and particularly in northern regions (Fig. 6c). Picoeukaryotes and green algae comprised the bulk of the  
15 remaining phytoplankton assemblage composition (generally  $< 10 \%$ ). In contrast to our observations for T1, DMS  
16 concentrations exhibited negative correlations to both salinity ( $r=-0.69$ ,  $p<0.001$ ; Fig. 6b) and SSHA ( $r=-0.81$ ,  $p<0.001$ ) in this  
17 area and were not significantly correlated to chl-*a* (Fig. 6c). Despite the lack of correlation to chl-*a*, DMS did exhibit  
18 significant, though weak, positive correlations with estimates of relative microphytoplankton abundance ( $r=0.22$ ,  $p<0.001$ ),  
19 and stronger negative correlations with the abundance of pico- and nano- size classes (T2:  $r=-0.47$ ,  $r=-0.45$ ;  $p<0.001$ ; Fig. 6c).  
20 In support of this observation, HPLC-pigment data from discrete sampling stations revealed a strong positive relationship  
21 between DMS concentration and relative abundance of diatoms ( $r=0.88$ ,  $p=0.001$ ), and a negative correlation between DMS  
22 and combined dinoflagellate and prymnesiophyte abundance ( $r=-0.88$ ,  $p=0.001$ ). These correlations suggest diatoms as an  
23 important source of DMS, in contrast to that observed for T1.

24  
25 Unlike bulk chl-*a* concentrations, we found that primary productivity showed a strong positive correlation with DMS along  
26 T2 ( $r=0.90$ ,  $p=0.037$ ), although this result is based on only four data points. Bacterial productivity was also significantly higher  
27 in the high DMS waters, although this variable was even more sparsely sampled along the transect, and we cannot infer any  
28 meaningful statistical association with DMS (Fig. 6f). As with T1, both  $k_{\text{DMSPd}}$  and  $k_{\text{DMS}}$  appeared higher in the low-DMS  
29 portions of the transect. Across the entire transect, DMS and DMSP consumption rate constants ranged from  $0.51$  to  $1.29 \text{ d}^{-1}$   
30 and  $28.8$  to  $49.5 \text{ d}^{-1}$ , respectively (Fig. 6e). This result suggests microbial consumption as potential driver of DMS  
31 distributions, with higher DMS/P consumption rate constants in waters with lower DMS concentrations.

32

1 Integrated biological DMS loss was significantly higher than that of T1, with an average  $78 \mu\text{mol m}^{-2} \text{d}^{-1}$  (equivalent to removal  
2 of 87 % of the DMS burden per day). By comparison, DMS sea-air flux across the transect was low, with a mean value of  $2.9$   
3  $\mu\text{mol m}^{-2} \text{d}^{-1}$ . This flux was sufficient to remove only  $\sim 6$  % of mixed layer DMS burden daily. We thus conclude that biological  
4 processes play a significant role in DMS turn-over along this transect.

### 5 **3.3.3 Transect 3**

6 T3 was located in the highly productive coastal waters of La Perouse Bank, along the continental shelf of the west coast of  
7 Vancouver Island (Fig. 1). DMS concentrations across this transect ranged from  $<1$ – $24$  nM, while DMSPd and DMSPp  
8 concentrations were among the highest observed cruise-wide ( $1.1$  –  $9.8$  nM and  $26$  –  $480$  nM, respectively; Fig. 7d). DMSPp  
9 was correlated to DMS ( $r=0.76$ ,  $p=0.02$ ). Mixed layer depths ranged from  $8$ – $12$  m, with the shallowest values found in fresher,  
10 salinity-stratified inshore waters influenced by riverine input. Sea surface temperature was lower in these low salinity waters,  
11 although it varied little over the transect (standard deviation  $< 1^\circ \text{C}$ ). With respect to other measured variables, DMS behaved  
12 similarly to the coastal T2 transect (Fig. 7a). We observed negative correlations between DMS and salinity ( $r=-0.78$ ,  $p<0.001$ ;  
13 Fig. 7b) and SSHA ( $r=-0.75$ ,  $p<0.001$ ). We also found elevated chl-*a* in the low salinity waters, although there was only a  
14 weak positive correlation between chl-*a* and DMS ( $r=0.25$ ,  $p<0.001$ ) across the full transect (Fig. 7c).

15

16 Microphytoplankton consisting primarily of diatoms dominated the low-salinity, high-DMS waters of the transect, with a shift  
17 towards smaller cells observed in the more saline waters farther offshore (Fig. 7c). Among the T3 stations, green algae,  
18 prokaryotes, and picoeukaryotes each comprised  $\sim 5$  –  $20$  % of phytoplankton abundance. Similar to T2, we found a significant  
19 positive correlation between DMS and microphytoplankton ( $r=0.90$ ,  $p<0.001$ ), and a negative correlation between DMS and  
20 phytoplankton of the nano- and pico- size class ( $r=-0.77$ ,  $r=-0.75$ ;  $p<0.001$ ). In support of this observation, HPLC-pigment  
21 data showed a strong positive relationship between DMS concentration and relative abundance of diatoms ( $r=0.94$ ,  $p<0.001$ ),  
22 and a negative correlation with combined dinoflagellate and prymnesiophyte abundance ( $r=-0.74$ ,  $p=0.023$ ). A negative  
23 relationship was also observed between DMSPp:chl-*a* and DMS ( $r=-0.88$ ,  $p=0.002$ ) (Fig. 7d). In contrast to T1, high DMS  
24 coincided with regions of lower cellular DMSP concentrations among phytoplankton, consistent with the dominance of  
25 diatoms in the high DMS portions of this transect.

26

27 Along the T3 transect, DMS exhibited a positive qualitative association with primary productivity and bacterial productivity,  
28 though these relationships are based on very few sampling points. It is noteworthy that the bacterial productivity measured  
29 along T3 was higher than anywhere else along the cruise track, with production more than 5-fold greater than the cruise-wide  
30 average. Values of  $k_{\text{DMS}}$  ranged from  $0.8$ – $2.7 \text{d}^{-1}$  across the transect. As with T1 and T2,  $k_{\text{DMS}}$  was higher in low-DMS regions  
31 of T3. In contrast,  $k_{\text{DMSPd}}$  values along T3 increased in parallel with DMS concentrations (higher rate constants in higher DMS  
32 waters). DMSP loss constants ranged from  $38.6$  to  $92.1 \text{d}^{-1}$  (Fig. 7e). The highest DMSP loss constant translates into a derived  
33 turnover time of just 16 minutes, and coincided with the highest bacterial productivity ( $\sim 26 \mu\text{g POC L}^{-1} \text{d}^{-1}$ ).

1  
2 Biological DMS loss integrated over the mixed layer was sufficiently high to remove >100 % of the DMS burden daily (~47  
3  $\mu\text{mol m}^{-2} \text{d}^{-1}$ ). By comparison, sea–air fluxes were a minor loss term by comparison ( $4.9 \mu\text{mol m}^{-2} \text{d}^{-1}$ ), and were sufficient to  
4 remove only ~12 % of the mixed layer DMS burden. Due to low removal rates and relative homogeneity of wind speed fields,  
5 sea–air flux cannot be invoked to explain the spatial distribution of DMS across this transect.

### 6 **3.4 Regional DMS distribution – comparisons of 2016 and 2017 observations with past studies**

7 To explore potential regional-scale relationships between DMS concentrations and other environmental variables, we  
8 combined our new DMS data with measurements collected over the past three decades, including previously unpublished high-  
9 resolution MIMS data. The addition of new measurements to the existing PMEL data set substantially increases spatial and  
10 temporal coverage in the NESAP. When data were binned to  $1^\circ \times 1^\circ$  resolution, coverage was increased by ~20 % in the  
11 CCAL and ALSK Longhurst provinces, and 14 % in the PSAE, with the overall addition of 90 data-containing grid cells (Table  
12 2). As shown in Fig. 8, our measurements primarily increase data coverage in waters below  $57^\circ \text{N}$ . These regions were  
13 previously under-sampled in the PMEL data set utilized by L11, which was strongly biased to measurements near the coast of  
14 Alaska. Figure 9a further illustrates the latitudinal shift in data coverage with the inclusion of additional MIMS data. As  
15 shown in Fig. 9b, average derived DMS concentrations across latitudinal bands at the north and south extremes of our study  
16 area remain similar to those derived from the PMEL data set utilized by L11. However, in the region between  $50^\circ \text{N}$  and  $54^\circ$   
17  $\text{N}$ , where there were few observations in the PMEL database, our compiled data show mean concentrations as much as  $4.5 \text{ nM}$   
18 (~40 %) lower than those calculated using PMEL data alone.

19  
20 Table 3 shows the change in province-wide average DMS concentration, sea–air fluxes, and total summertime DMS flux based  
21 on our updated analysis. Relative to our revised estimates, DMS concentrations and sea-air fluxes derived using only the  
22 PMEL data were lower in the CCAL and higher in both the PSAE and ALSK provinces. The most pronounced difference was  
23 that of sea–air flux in the PSAE, where estimated values decreased by  $4.5 \mu\text{mol m}^{-2} \text{d}^{-1}$  (20 %). Despite these regional  
24 differences, the total summer DMS flux across the NESAP differed by only 6.5 % between our compiled data set ( $0.30 \text{ Tg S}$ )  
25 and the PMEL data set utilized by L11 ( $0.32 \text{ Tg S}$ ).

26  
27 Our compiled data set provides greater confidence in DMS concentrations and sea–air fluxes across the NESAP, and enables  
28 us to better constrain spatial patterns. Figure 10 shows binned average summertime DMS concentration across the region, as  
29 well as the derived sea–air DMS fluxes. The highest concentrations were observed in ALSK, where coastal waters contain  
30 maximum DMS concentrations exceeding  $20 \text{ nM}$ . A persistent region of elevated DMS concentrations was also evident in  
31 mid-PSAE oceanic region, with concentrations greater than  $10 \text{ nM}$ . Sea–air DMS fluxes showed a spatial distribution similar

1 to DMS concentrations, with maximum values of  $>100 \mu\text{mol m}^{-2} \text{d}^{-1}$ . Calculated DMS:chl-*a* ratios for binned data (Fig. 10c),  
2 showed generally higher values in offshore NESAP waters.

### 3 **3.5 Correlations and algorithm testing**

4 Using our new data compilation, we examined the relationship between DMS concentrations and a suite of oceanographic  
5 variables across the NESAP. Table 4 shows both NESAP-wide and province-specific correlations derived from this analysis.  
6 While many correlations are weak or not statistically significant, some patterns do emerge, particularly in the offshore waters  
7 of the PSAE domain. No single variable explains a large portion of the DMS variation in this province, but statistically  
8 significant correlations exist between DMS and chl-*a* and calcite ( $r=0.45$  and  $r=0.50$ , respectively). We also found a negative  
9 relationship between DMS and SSHA ( $r=-0.47$ ). For the ALSK province, we found weak inverse correlations between DMS  
10 and SST ( $r=-0.32$ ) and water depth ( $r=-0.34$ ). Significant positive correlations between DMS and derived surface  $\text{NO}_3$   
11 concentrations, PAR, and chl-*a* are also observed ( $r=0.30$ ,  $r=0.41$ , and  $r=0.34$  respectively). In contrast to other provinces, we  
12 observed a statistically significant correlation between DMS and NCP in the CCAL province ( $r=0.43$ ). The lack of other  
13 significant correlations in the province may, in part, reflect the lower number of data points obtained for this region.

14  
15 Moving beyond simple pairwise correlations, multi-variate empirical algorithms provide an additional approach to assess the  
16 potential drivers of regional DMS dynamics. We evaluated the ability of five previously published algorithms to reproduce  
17 patterns in the DMS observations. In order to obtain the best possible results, we modified the original equations using a least  
18 squares method to obtain the best-fit coefficients for our data set. We evaluated the algorithm outputs against observations  
19 using Pearson's correlation coefficients and root mean square errors (RMSE). As shown in Table 5, model performance was  
20 generally low, with most correlation coefficients less than 0.53 and RMSE values ranging from 1.2 to 81.6 nM. The best  
21 results were obtained for the CCAL province, where both the tuned SD02 and the original G18 algorithms were able to predict  
22 DMS concentrations with moderate success ( $r = 0.62^*$ , RMSE = 1.61 and  $r = 0.72^*$ , RMSE = 1.9, for SD02 and G18,  
23 respectively). As both of these algorithms rely on MLD, which is only available for waters deeper than 2000 m, it is important  
24 to note that predictive strength can only be assessed for these off-shelf waters, and should not be taken to represent performance  
25 in coastal waters. The customized VS07 (with coefficients tuned to the NESAP data) showed the best overall performance  
26 across the entire NESAP region. Yet, even this model showed only weak correlation between predicted and observed DMS  
27 values ( $r=0.31$ ). Notably, the original linear coefficients for this model yielded DMS concentrations that were inversely  
28 correlated to the measured values. In no case did models using original linear coefficients outperform those using recalculated  
29 coefficients.



## 1 **4 Discussion**

2 The results presented here provide new information on the fine-scale and regional patterns of DMS distributions across the  
3 NESAP. Our ship-board observations document sub-mesoscale variability in DMS concentration across hydrographic frontal  
4 zones, with associated process measurements providing insight into potential driving factors. By combining these new data  
5 with more than three decades of DMS measurements, we are able to improve data coverage for the NESAP to examine larger-  
6 scale spatial patterns and provide a more robust regional climatology to evaluate empirical predictive algorithms.

### 7 **4.1 Contrasting cycling regimes within the NESAP**

8 A number of studies have documented differences in DMS dynamics across oceanographic regimes in the NESAP (Royer et  
9 al. 2010, Asher et al. 2011, 2017). These regional differences result from complex ecosystem and environmental interactions,  
10 and limit broad-scale prediction of DMS concentrations and sea–air fluxes (Galí et al. 2018). Taxonomic composition of  
11 phytoplankton assemblages has been identified as a main driver of DMS distribution patterns. For example, dinoflagellates  
12 and prymnesiophytes typically have elevated DMS production, associated with greater intracellular concentrations of DMSP  
13 (Keller 1989) and, in some cases, high activity of DMSP lyase (the enzyme that cleaves DMSP to DMS and acrylate; Steinke  
14 et al. 2002; Wolfe et al. 2002; Curson et al. 2018). In contrast, bloom-forming diatom species have typically lower intracellular  
15 DMSP levels (Keller 1989), with the exception of some polar species (Levasseur et al. 1994, Matrai and Vernet 1997).  
16 However, nutrient limitation has been shown to significantly increase diatom DMS/P production (Bucciarelli and Sunda 2003;  
17 Sunda et al. 2007; Harada et al. 2009). Thus, the accumulation of DMS in the water column depends on both the composition  
18 of phytoplankton assemblages and their physiological state, as previously shown by Gabric et al. (1999). Other factors,  
19 including zooplankton grazing and the metabolic demands of heterotrophic bacteria are also important (e.g. Levasseur et al.  
20 1996, Kiene and Linn 2000, Merzouk et al. 2006, Asher et al. 2017). Below, we discuss the potential factors driving high  
21 DMS concentrations along three frontal zones exhibiting sharp DMS concentration gradients. Specifically, we contrast the  
22 nanoplankton dominated T1 transect with the diatom-dominated coastal T2 and T3 transects, examining the environmental  
23 and biological conditions that may have led to the different DMS accumulation in these areas.

### 24 **4.2 The importance of phytoplankton assemblage composition**

25 The T1 transect, located in the southern-most portion of the ALSK province, spanned 5° of longitude from deep (>3000 m)  
26 offshore waters, into nearshore waters over the continental shelf. These oceanographic regimes were separated by strong  
27 hydrographic frontal features in the vicinity of the shelf break. The negative correlation between DMS and chl-*a* along this  
28 transect demonstrates that DMS accumulation did not directly scale with bulk phytoplankton biomass. Rather, our results  
29 suggest that DMS concentrations were likely influenced by phytoplankton assemblage composition, with the highest DMS  
30 concentrations associated with the greatest relative proportion of prymnesiophytes and dinoflagellates (Fig. 4c) and the highest  
31 DMSP:chl-*a* (Fig. 4d). Similar relationships have been documented in numerous studies focusing on offshore waters of the

1 NESAP and elsewhere (e.g. Barnard et al. 1984; Hatton et al. 1999; Royer et al. 2010; Steiner et al. 2012). In these areas,  
2 elevated DMS concentrations are often attributed to a preponderance of high-DMSP phytoplankton taxa.  
3  
4 Comparison of T2 and T3 with T1 shows that the association of elevated DMS with prymnesiophyte and dinoflagellate  
5 dominance and high DMSPp:chl-*a* ratios did not hold across our entire survey region. As was observed by Royer et al. (2010),  
6 we measured generally low DMSPp:chl-*a* ratios in the diatom-dominated coastal waters of T2 and T3 (Fig. 6d, 7d). Yet, DMS  
7 concentrations measured in these waters were extremely high, at times exceeding 20 nM (Fig. 2a). Unlike the T1 transect,  
8 DMS concentrations along T2 and T3 increased with decreasing DMSPp:chl-*a* ratios, and were strongly correlated with diatom  
9 abundance.  
10  
11 One potential explanation for the difference between T1 and T2/T3 may relate to the different location of these sampling  
12 regions. The T1 transect sits along the transition between offshore and inshore waters, where different nutrient regimes control  
13 phytoplankton productivity. Inshore waters over the continental shelf are typically limited by macronutrients, whereas offshore  
14 waters transition into iron-limitation (Boyd and Harrison 1999). At the boundary between these regimes, mixing of water  
15 masses through horizontal advection can stimulate phytoplankton productivity (Lam and Letters 2008). Ribalet et al. (2010)  
16 observed an active community of nanoplankton in the transitional waters, and attributed this to the stimulation of (often high-  
17 DMSP) oceanic phytoplankton by water mass mixing, at the boundary of macro- and micro-nutrient rich waters.  
18 Formation of Haida and Sitka eddies may aid in this mixing through the westward transportation of micronutrient-replete  
19 coastal water (Johnson et al. 2005; Whitney et al. 2005). SSHa measurements can be used as an indicator of eddy-induced  
20 mixing in this region, as warm-core Haida and Sitka eddies waters manifest as closed circulation features exhibiting positive  
21 SSHa (Fig. 1c, d). We observed the highest DMS associated with positive SSHa along T1 (Fig. 5), suggesting the influence  
22 of water mass mixing in driving mesoscale patterns of DMS distribution. Beyond this mesoscale coherence, unresolved sub-  
23 mesoscale variability is likely attributable to biological heterogeneity (Fig. 4c, d; Royer 2015 et al.)  
24  
25 In contrast to the transition waters, nearshore waters over the continental shelf are typically dominated by low DMSP-  
26 producing diatoms. Elevated DMS in these diatom-rich waters may reflect a combination of high absolute biomass and an  
27 upregulation of DMSP production observed under nutrient stress (Bucciarelli and Sunda 2003; Sunda et al. 2007; Hockin et  
28 al. 2012; Bucciarelli et al. 2013). A meta-analysis by McParland and Levine (2018) reported an average 12-fold upregulation  
29 of intracellular DMSP production under nutrient-stress conditions among phytoplankton, including diatoms, typically  
30 considered low-producers. By comparison, high DMSP producers only showed an average 1.4-fold upregulation. Our results  
31 are similar to those of Barnard et al. (1984), who observed a decreasing influence of prymnesiophyte abundance on DMS  
32 concentrations in the Bering Sea with increasing proximity to the continental shelf. We note that increases in  
33 microphytoplankton abundances are often accompanied by increases in other phytoplankton groups (including high-DMSP  
34 producing taxa; Barber and Hiscock 2006; Uitz et al. 2006). However, we observed no correlation between DMS and the

1 absolute abundance of prymnesiophytes and dinoflagellates for either T2 or T3 transects. This result suggests that while these  
2 high-DMSP producing taxa may play a role in driving DMS concentrations along these transect, diatoms are likely dominant  
3 contributors, as judged by the strong correlation between DMS and absolute diatom absolute abundance ( $r=0.91$ ,  $p=0.001$ )  
4 along T3.

5  
6 In coastal waters, seasonal upwelling may drive high phytoplankton biomass accumulation and increased DMS production in  
7 the late-bloom phase, when stratified surface layers are exposed to higher mean light intensities (due to shallow mixing) and  
8 become nutrient depleted (Zindler et al. 2012). These environmental conditions would act to increase cellular oxidative stress,  
9 thus promoting the production of DMS/P as part of a cellular response mechanism (Sunda et al. 2002). Further, several studies  
10 have shown increased bacterial activity and higher rates of cellular DMSP leakage in the late-bloom phase (Malin et al. 1993;  
11 Stefels and Boekel 1993; Matrai and Keller 1994). The results of Asher et al. (2017) demonstrating high DMS concentrations  
12 in post-upwelling waters of the coastal NESAP support this idea. Measurements of SSHA in coastal regions can provide a  
13 signature for recent upwelling; the combined effect of wind-induced seasonal water transport offshore and the presence of high  
14 density (cold and saline) upwelled water acts to depress sea surface height relative to annual means (Smith 1974; Tabata et al.  
15 1986; Strub and James 1995; Saraceno et al. 2008; Venegas et al. 2008). Negative relationships between DMS concentrations  
16 and SSHA were observed in both the T2 and T3 transects, suggesting an association between DMS and upwelling events.

17  
18 Additional ecosystem processes may influence DMS accumulation in surface waters. In particular, zooplankton grazing and  
19 viral infection may increase DMS concentrations, due to the release of cellular DMSP in phytoplankton during sloppy feeding  
20 and cellular lysis (Dacey and Wakeham 1986; Belviso et al. 1990; Hill et al. 1998). Both of these factors are density-dependent,  
21 and thus likely to become more significant with higher phytoplankton cell densities in the late bloom phase. Unfortunately,  
22 we do not have measurements to address these processes directly, but the elevated DMSPd concentrations along T3 (~7 nM)  
23 may reflect viral and zooplankton mediated loss of particulate DMSP into the dissolved pool.

24  
25 Taken together, our results support previous studies showing the importance of DMSP-rich species in driving high DMS  
26 concentration in offshore waters of the NESAP and elsewhere (e.g Stefels et al. 2007, Royer et al. 2010, Steiner et al. 2012,  
27 Asher et al. 2017). In coastal waters, it appears that diatom-dominated phytoplankton assemblages can also support elevated  
28 DMS accumulation, particularly under high biomass conditions during the late bloom phase, as has been previously observed  
29 in the Southern Ocean (Turner et al. 1995) and the Barents Sea (Matrai and Vernet 1997).

### 30 **4.3 The effect of DMS/P consumption rate on DMS distribution**

31 DMS consumption rates constants across our study area can be translated to biological DMS turnover times ranging from 9 h  
32 to 2.5 d (average of 25 h). By comparison, turnover times calculated from sea–air flux removal rates averaged 6.1 d across  
33 this area, suggesting that this term is less important in the mixed layer DMS budget. We note that DMS concentration is set

1 by the dynamic balance between production and loss terms (Galí and Simó, 2015), of which only a subset were measured in  
2 our study. Gross DMS production, DMS production from DMSP cleavage, and DMS loss from photo-oxidation, which we  
3 did not measure, constitute potentially important terms in driving DMS distribution. Further, our conclusions are limited by  
4 data coverage, and based, at times, on few measurements. Notwithstanding these limitations, to our knowledge, no study has  
5 yet assessed DMS/P turnover rates across frontal zones on the small spatial scales examined here. Our limited measurements  
6 thus remain important in comparing meso- and submesoscale processes to those operating on larger spatial scales. While these  
7 measures do not encompass all loss processes, we found that biological consumption and sea–air flux alone were sufficient to  
8 quickly erase a DMS accumulation signature in the mixed layer. Thus, DMS concentrations measured here appear to be  
9 reflective of short-term production and consumption processes.

10

11 Across our study area, biological DMS removal rate constants ( $d^{-1}$ ) were inversely related to DMS concentrations ( $r=-0.55$ ,  
12  $p=0.03$ ), with lower  $k_{DMS}$  in waters with elevated DMS. This study-wide trend supports the relationships observed along each  
13 transect. The relationship may reflect a time-lag of bacterial response to increased DMS concentrations. Results from previous  
14 studies in other regions have shown that bacterial DMS consumption increases after a rapid rise in DMS concentrations,  
15 resulting in consumption rate constants that are relatively low when DMS concentrations are initially high. As consumption  
16 rate constants increase, DMS concentrations decrease (Zubkov et al. 2004; del Valle et al. 2009). These results, along with  
17 the observed positive correlation between DMS and bacterial activity ( $r=0.53$ ,  $p=0.03$ ), suggest that microbial consumption is  
18 an important control on DMS accumulation, irrespective of phytoplankton community assemblage. However, the positive  
19 correlation between DMS loss rates and concentrations suggests that microbial consumption may not be sufficient to offset  
20 new DMS production. Previous studies in other regions have examined the impact of DMS loss and production in driving  
21 distributions, demonstrating correlations between DMS concentrations and microbial consumption and production rates in  
22 some systems (Wolfe and Kiene 1993; Zubkov et al. 2002 Merzouk et al. 2006, Vila-Costa et al. 2008). The relationship  
23 observed here between DMS,  $k_{DMS}$  and bacterial activity may reflect the preponderance of on-shelf stations measured for DMS  
24 consumption in our survey (10 out of 16 stations), and significantly higher rates of bacterial metabolism in onshore waters  
25 ( $7.81 \pm 3.0$  vs  $1.10 \pm 0.3$   $\mu\text{g POC L}^{-1} \text{d}^{-1}$  for on- and off-shelf stations, respectively).

26

27 Recent studies in the NESAP have estimated that photo-oxidation may account for 20–70 % of gross DMS removal in the  
28 NESAP (Asher et al. 2017), and it is possible that this process is particularly important in offshore waters. Bouillon and Miller  
29 (2004) found that quantum yields of DMS photo-oxidation in the NESAP correlated well to nitrate concentrations, suggesting  
30 that this pathway is particularly relevant in the HNLC region where excess macronutrients persist throughout the summer.  
31 Thus, the role of biological DMS consumption on influencing total DMS concentrations may be more important in the  
32 generally low nitrate coastal waters.

33

1 Rates of DMSPd turnover were among the highest measured anywhere, likely due, in part, to the very high productivity of the  
2 waters we sampled. However, no correlation was found between DMSPd loss rates or loss rate constants and DMS  
3 concentrations in our study. This lack of correlation may be due, in part, to variation in DMSPd loss pathways. The DMS  
4 yield of DMSP metabolism can vary significantly depending on metabolic needs of bacteria present, and relative abundance  
5 of phytoplankton with DMSP lyase activity (Yoch 2002). Although DMS yield was not measured in this study, previous  
6 reports have shown that in the NESAP, a low carbon to organic sulfur ratio in the HNLC regime results in increased DMS-  
7 yield from DMSP metabolism, whereas onshore DMS-yield is relatively lower (Merzouk et al. 2006; Royer et al. 2010).  
8 Further, variation in DMS loss processes may obscure a relationship between DMSPd cleavage and DMS concentrations, as  
9 high loss terms may disproportionately impact net DMS production. We are currently investigating, in greater detail, the  
10 patterns of DMS and DMSPd consumption from our O16 and O17 cruises (Kiene et al., in prep).

#### 11 **4.4 Insights from merged data set**

12 Our merged data set, binned to  $1^\circ \times 1^\circ$  spatial resolution, builds on the L11 climatology to further constrain summertime DMS  
13 distributions across the NESAP region. Despite an overall ~20 % increase in data-containing bins, and the inclusion of data  
14 from seven additional years, we see only small changes in the derived climatological DMS concentrations and sea–air fluxes  
15 when compared to the PMEL data set used by L11 (Table 3). Our new observations thus support the validity of the L11  
16 climatology in the NESAP region, providing further confidence in the apparent distribution patterns, and a greater spatial  
17 footprint for the climatological field. A significant result of our analysis is the presence of high DMS:chl-*a* in offshore waters  
18 (Fig. 10c). This result builds on previous reports of higher DMSP:chl-*a* concentrations in offshore NESAP waters, and  
19 highlights the importance of prymnesiophytes, dinoflagellates, and other DMSP-rich phytoplankton taxa in driving DMS  
20 accumulation in this region.

#### 21 **4.5 Biogeochemical provinces**

22 When examining results from our  $1^\circ$  binned data set, a separation of the NESAP into on- and off-shelf regimes does not capture  
23 the biogeochemical complexities of the region. Ecological provinces, as defined by Longhurst (2007), define regions with  
24 coherent seasonal trends in physical processes, which give rise to similar biological and chemical characteristics. The use of  
25 Longhurst’s biogeochemical provinces may thus be a more suitable (though still imperfect) approach to examine large-scale  
26 and long-term differences in DMS cycling across the region. Work by Reygondeau et al. (2013) has demonstrated the potential  
27 for shifts in province boundaries over time, including decrease of coastal province size during El Nino periods, and a general  
28 shore-ward shift of ALSK boundaries during summer months. A model-based classification of marine ecosystems in the North  
29 Pacific by Gregr and Bodtker (2007) divides our study region into six domains that show little similarity to Longhurst  
30 provinces. It is difficult to say which of these classification schemes is most appropriate for examination of DMS dynamics.  
31 However, for the sake of direct comparison with L11, we chose to use Longhurst’s provinces to examine regional cycling  
32 differences (Hind et al. 2011; Belviso et al. 2011; Royer et al. 2015). While we acknowledge these provinces provide only a

1 crude distinction of biogeochemical regimes, they remain a best-approximation without delving into more complicated time-  
2 resolved ecological province models (Reygondeau et al. 2013). Going forward, it may be useful to examine DMS dynamics  
3 in sub-regions defined with a number of different metrics.

#### 4 **4.6 Correlation with environmental variables**

5 Our analysis shows that no single variable can explain an appreciable amount of variability in DMS concentrations across the  
6 NESAP. This result is consistent with previous global and regional studies (Kettle et al. 1999; Vézina 2004; Lana et al. 2011).  
7 Nonetheless, an examination of the differing relationships between DMS concentrations and other environmental variables  
8 provides insight into potential underlying factors driving DMS distribution (Table 4). For example, although we found a  
9 moderately strong significant positive correlation between DMS and chl-*a* in the largely HNLC PSAE province, no relationship  
10 was observed between these variables in the CCAL province. As noted above and confirmed in several previous studies, the  
11 phytoplankton community structure in the offshore PSAE region consists largely of small, DMSP-rich species (Booth et al.  
12 1993; Suzuki et al. 2002; Royer et al. 2010; Steiner et al. 2012), and large blooms are infrequent. Indeed, the average binned  
13 chl-*a* concentration in this province is  $< 1 \mu\text{g L}^{-1}$ . As such, modest increases chl-*a* likely reflects a stimulation of this high  
14 DMSP-producing community. The positive correlation with calcite (an indicator of high-DMSP producing coccolithophores)  
15 supports this idea.

16  
17 The relationship between chl-*a* and DMS is more complicated in the CCAL. High productivity in coastal upwelling zones  
18 results in a strong onshore/offshore trend in average chl-*a* concentrations. Yet, no such trend is observed in DMS  
19 concentrations. This may be due, in part, to the sensitivity of DMS concentrations to phytoplankton assemblage composition  
20 and bloom dynamics. High phytoplankton biomass alone will not result in elevated DMS in this region. Rather, elevated  
21 DMS concentrations may occur as a response to conditions of late-bloom nutrient stress, as discussed above and in section 4.7.

22  
23 Factors driving observed DMS distribution patterns in the ALSK province are more difficult to surmise. DMS is notably high  
24 in the cold, productive waters adjacent to the Alaskan Peninsula. This is affirmed by a weak negative correlation between  
25 DMS and SST, and the positive correlation between DMS and chl-*a*. Given that this portion of the province is known to  
26 experience localized summer upwelling, it is possible that high DMS in the regions simply reflects elevated productivity and  
27 related upwelling-induced stressors.

#### 28 **4.7 Algorithm performance**

29 Our results suggest that no single empirical algorithm is likely to perform well in predicting DMS distributions across the  
30 subarctic Pacific, although some predictive success was observed in the offshore waters of the CCAL province. Perhaps the  
31 most informative result was the negative correlation between measured and modelled results using the VS07 algorithm. This  
32 algorithm predicts DMS concentrations from solar radiative dose, a term that measures depth-integrated exposure to sunlight.

1 The underlying assumption in this algorithm is that increases in SRD are accompanied by increases in DMS due to UV-induced  
2 oxidative stress (Vallina and Simó 2007). However, it is also possible that elevated SRD can also lead to a decrease in surface  
3 water DMS concentrations through DMS photo-oxidation. As observed in previous studies, photo-oxidation in the NESAP  
4 may account for up to 70 % of gross DMS removal, and rates are positively correlated with nitrate concentrations (Bouillon  
5 and Miller 2004; Asher et al. 2017). Thus, in the high-nitrate NESAP, SRD may serve primarily to remove DMS from surface  
6 waters, rather than stimulate DMS production, as suggested by the negative correlation between DMS and SRD across the  
7 NESAP and within the PSAE province (Table 5). In areas with low surface water nitrate concentrations, such as the CCAL  
8 province (Boyd and Harrison 1999), SRD could act to promote DMS accumulation. The good performance of the G18  
9 algorithm in the CCAL province supports this idea. In contrast to the VS07 algorithm, G18 includes terms representing both  
10 irradiance (PAR) and biology (DMSPt estimate), thus including the influence the combined effect of biomass and  
11 phytoplankton physiological state. The poor performance of the G18 algorithm across other NESAP regions may be due to  
12 the nitrate–photolysis relationship described above, or to the limited environmental-dependence of DMSP production in  
13 prymnesiophyte / dinoflagellate-dominated HNLC phytoplankton (McParland and Levine 2018).

14

15 The results discussed above underline the need for regional algorithm tuning, and the selection of models best suited for a  
16 given area and season. There is a particular need to develop approaches representing DMS distributions in HNLC regions. In  
17 order to accomplish this goal, it will be important to improve mechanistic understanding of DMS/P dynamics, merging field-  
18 based process studies with prognostic numerical models (e.g. Aumont et al. 2002, Clainche et al. 2004, Steiner et al. 2012,  
19 Wang et al. 2015, Hayashida et al. 2016).

## 20 **5 Conclusion**

21 This study examines the distribution and cycling of DMS across the NESAP at various spatial scales. Our results confirm the  
22 importance of high-DMSP producers (i.e. prymnesiophytes and dinoflagellates) to DMS accumulation in offshore waters,  
23 while also demonstrating the importance of diatom-dominated assemblages in driving DMS distribution in coastal upwelling  
24 regions. We further highlight the importance of metabolic rate processes in DMS distributions, providing evidence for the  
25 importance of DMS consumption on concentration gradients at a fine-scale. On the short spatial scales covered by our transect  
26 surveys, we observed strong correlations between DMS concentrations and other variables (i.e. SSHA, salinity). Over regional  
27 scales, however, we only observed weak statistical relationships. All predictive algorithms we tested showed poor performance  
28 in predicting DMS concentrations across the NESAP region, although performance was improved through the use of  
29 regionally-tuned coefficients. Our compiled data set further support the importance of the NESAP as a global DMS ‘hot spot’  
30 in summer, with patterns of DMS concentrations and sea–air fluxes similar to those observed in Lana et al.’s 2011 climatology.  
31 Given the significance of the NESAP in global oceanic DMS emissions, future studies should seek to improve mechanistic

1 understanding of the factors driving DMS accumulation in this region, with the aim of predicting climate-dependent changes  
2 over the coming decades.

### 3 **Code availability**

4 The codes used for spatial binning and data analysis can be provided by the authors upon request.

### 5 **Data availability**

6 All previously publicly unavailable DMS concentration data presented here have been submitted to the NOAA PMEL database  
7 (<http://saga.pmel.noaa.gov/dms/>). Ancillary shipboard and satellite data can be provided by the authors upon request.

### 8 **Author contributions**

9 A. Herr compiled and analysed all data presented here, wrote all MATLAB codes, and wrote the manuscript, with editing and  
10 intellectual input provided by P. Tortell R. Kiene and J. Dacey. R. Kiene further provided all biological rate measurement  
11 data presented here, and J. Dacey assisted in collection of other field measurements.

### 12 **Competing interests**

13 The authors declare that they have no conflict of interest.

### 14 **Acknowledgements**

15 We dedicate this article to the memory of Dr. Ron Kiene, a wonderful scientist, mentor and friend. His contributions to DMS/P  
16 research have shaped our field over the past three decades, and he will be missed by many around the world. We also wish to  
17 thank many individuals involved in data collection and logistical aspects of the cruises presented here, including scientists  
18 from the Institute of Ocean Sciences, the captain and crew of the R/V *Oceanus* and the CCGS *John P. Tully*, and members  
19 Tortell, Kiene, Levine and Hatton laboratory groups. We also thank T. Ahlvin for GIS support, and both reviewers for their  
20 insightful comments. Support for this work was provided from the US National Science Foundation (Grant #1436344), and  
21 from the Natural Sciences and Engineering Research Council of Canada.



## 1 **References**

- 2 Asher, E. C., Merzouk, A., and Tortell, P. D.: Fine-scale spatial and temporal variability of surface water dimethylsulfide  
3 (DMS) concentrations and sea–air fluxes in the NE Subarctic Pacific, *Mar. Chem.*, 126, 63–75,  
4 doi:10.1016/j.marchem.2011.03.009, 2011.
- 5
- 6 Asher, E. C., Dacey, J. W. H., Jarníková, T., Tortell, P. D.: Measurement of DMS, DMSO, and DMSP in natural waters by  
7 automated sequential chemical analysis, *Limnol. Oceanogr.-Methods*, 13, 451–462, doi: 10.1002/lom3.10039, 2015.
- 8
- 9 Asher, E., Dacey, J. W., Ianson, D., Peña, A., and Tortell, P.D.: Concentrations and cycling of DMS, DMSP, and DMSO in  
10 coastal and offshore waters of the Subarctic Pacific during summer, 2010-2011, *J. Geophys. Res.-Oceans*, 122(4), 3269–3286,  
11 doi:10.1002/2016JC012465, 2017.
- 12
- 13 Aumont, O., Belviso, S., and Monfray, P.: Dimethylsulfoniopropionate (DMSP) and dimethylsulfide (DMS) sea surface  
14 distributions simulated from a global three-dimensional ocean carbon cycle model, *J. Geophys. Res.-Oceans*, 107, 3029,  
15 doi:10.1029/1999JC000111, 2002.
- 16
- 17 Balch, W. M., Gordon, H. R., Bowler, B. C., Drapeau, D. T., and Booth, E. S.: Calcium carbonate measurements in the surface  
18 global ocean based on Moderate-Resolution Imaging Spectroradiometer data, *J. Geophys. Res.-Oceans*, 110, C07001,  
19 doi:10.1029/2004JC002560, 2005.
- 20 Barber, R. T. and Hiscock, M. R.: A rising tide lifts all phytoplankton: Growth response of other phytoplankton taxa in diatom-  
21 dominated blooms, *Global Biogeochem. Cycles*, 20, 1–12, doi:10.1029/2006GB002726, 2006.
- 22 Barnard, W. R., Andreae, M. O., and Iverson, R. L.: Dimethylsulfide and *Phaeocystis poucheti* in the southeastern Bering Sea,  
23 *Cont. Shelf Res.*, 3, 103–113, doi: 10.1016/0278-4343(84)90001-3, 1984.
- 24
- 25 Belviso, S., Kim, S.-K., Rassoulzadegan, B., Krajka, B., Nguyen, B. C., Mihalopoulos, N., and Buat-Menard, P.: Production  
26 of dimethylsulfonium propionate (DMSP) and dimethylsulfide (DMS) by a microbial food web, *Limnol. Oceanogr.* 35, 1810–  
27 1821, doi: 10.4319/lo.1990.35.8.1810, 1990.
- 28 Belviso, S., Sciandra, A. and Copin-Montégut, C.: Mesoscale features of surface water DMSP and DMS concentrations in the  
29 Atlantic Ocean off Morocco and in the Mediterranean Sea, *Deep. Res. Part I Oceanogr. Res. Pap.*, 50, 543–555,  
30 doi:10.1016/S0967-0637(03)00032-3, 2003.

- 1 Belviso, S., Masotti, I., Tagliabue, A., Bopp, L., Brockmann, P., Fichot, C., Caniaux, G., Prieur, L., Ras, J., Uitz, J., Loisel,  
2 H., Dessailly, D., Alvain, S., Kasamatsu, N., and Fukuchi, M.: DMS dynamics in the most oligotrophic subtropical zones of  
3 the global ocean, *Biogeochemistry*, 110, 215–241, doi:10.1007/s10533-011-9648-1, 2012.
- 4
- 5 Booth, B., Lewin, J., and Postel, J.: Temporal variation in the structure of autotrophic and heterotrophic communities in the  
6 subarctic Pacific, *Prog. Oceanogr.*, 32, 57–99, doi:10.1016/0079-6611(93)90009-3, 1993.
- 7
- 8 Bouillon, R.-C., and Miller, W. L.: Determination of apparent quantum yield spectra of DMS photo-degradation in an in situ  
9 iron-induced Northeast Pacific Ocean bloom, *Geophys. Res. Lett.*, 31, L06310, doi:10.1029/2004GL019536, 2004.
- 10
- 11 Boyd, P. J. and Harrison, P. J.: Phytoplankton dynamics in the NE subarctic Pacific, *Deep-sea Res. Pt. I.*, 46, 2405–2432,  
12 doi:10.1016/S0967-0645(99)00069-7, 1999.
- 13
- 14 Boyd, P. W., Law, C. S., Wong, C. S., Nojiri, Y., Tsuda, A., Levasseur, M., Takeda, S., Rivkin, R., Harrison, P. J., Strzepek,  
15 R., Gower, J., McKay, M., Abraham, E., Arychuk, M., Barwell-Clarke, J., Crawford, W., Crawford, D., Hale, M., Harada, K.,  
16 Johnson, K., Kiyosawa, H., Kudo, I., Marchetti, A., Miller, W., Needoba, J., Nishioka, J., Ogawa, H., Page, J., Robert, M.,  
17 Saito, H., Sastri, A., Sherry, N., Soutar, T., Sutherland, N., Taira, Y., Whitney, F., Wong, S.-K. E., and Yoshimura, T.: The  
18 decline and fate of an iron-induced subarctic phytoplankton bloom, *Nature* 428, 549–553, doi:10.1038/nature02412, 2004.
- 19
- 20 Brewin, R., Sathyendranath, S., Hirata, T., Lavender, S., Barciela, R., and Hardman-Mountford, N.: A three-component model  
21 of phytoplankton size class for the Atlantic Ocean, *Ecol. Model.*, 221, 1472–1483, doi:10.1016/j.ecolmodel.2010.02.014,  
22 2010.
- 23
- 24 Bricaud, A., Babin, M., Morel, A. and Claustre, H.: Variability in the chlorophyll-specific absorption coefficients of natural  
25 phytoplankton: Analysis and parameterization, *J. Geophys. Res.-Oceans*, 100, 13321–13332, doi:10.1029/95JC00463, 1995.
- 26
- 27 Bucciarelli, E., and Sunda, W.: Influence of CO<sub>2</sub>, nitrate, phosphate, and silicate limitation on intracellular  
28 dimethylsulfoniopropionate in batch cultures of the coastal diatom *Thalassiosira pseudonana*, *Limnol. Oceanogr.*, 48, 2256–  
29 2265, doi:10.4319/lo.2003.48.6.2256, 2003.
- 30
- 31 Bucciarelli, E., Ridame, C., Sunda, W., Dimier-Hugueney, C., Cheize, M., and Belviso, S.: Increased intracellular  
32 concentrations of DMSP and DMSO in iron-limited oceanic phytoplankton *Thalassiosira oceanica* and *Trichodesmium*  
33 *erythraeum*, *Limnol. Oceanogr.*, 58, 1667–1679, doi:10.4319/lo.2013.58.5.1667, 2013.
- 34

- 1 Burt, W., Westberry, T., Behrenfeld, M., Zeng, C., Izett, R., Tortell, P.: Carbon: Chlorophyll Ratios and Net Primary  
2 Productivity of Subarctic Pacific Surface Waters Derived From Autonomous Shipboard Sensors, *Global Biogeochem. Cy.*, 32,  
3 267–288, doi:10.1002/2017GB005783, 2018.
- 4
- 5 Charlson, R. J., Lovelock, J. E., Andreae, M. O. and Warren, S. G.: Oceanic phytoplankton, atmospheric sulphur, cloud albedo  
6 and climate, *Nature*, 326, 655–661, doi:10.1038/326655a0, 1987.
- 7
- 8 Clainche, Y. L., Levasseur, M., Vézina, A., Dacey, J. W. H., and Saucier, F. J.: Behaviour of the ocean DMS (P) pools in the  
9 Sargasso Sea viewed in a coupled physical-biogeochemical ocean model, *Can. J. Fish. Aquat. Sci.*, 61, 788–803,  
10 doi:10.1139/F04-027, 2004.
- 11
- 12 Crawford, W., Brickley, P., Peterson, T., and Thomas, A.: Impact of Haida Eddies on chlorophyll distribution in the Eastern  
13 Gulf of Alaska, *Deep-Sea Res. Pt. II*, 52, 975–989, doi:10.1016/j.dsr2.2005.02.011, 2005.
- 14
- 15 Curson, A., Williams, B., Pinchbeck, B., Sims, L., Martínez, A., Rivera, P., Kumaresan, D., Mercadé E., Spurgin, L., Carrión  
16 O., Moxon S., Cattolico, R., Kuzhiumparambil, U., Guagliardo, P., Clode, P., Raina, J.-B., and Todd, J.: DSYB catalyses the  
17 key step of dimethylsulfoniopropionate biosynthesis in many phytoplankton, *Nat. Microbiol.*, 3, 430–439,  
18 doi:10.1038/s41564-018-0119-5, 2018.
- 19
- 20 Dacey, J. W., and Blough, N. V.: Hydroxide decomposition of dimethylsulfoniopropionate to form dimethylsulfide, *Geophys.*  
21 *Res. Lett.*, 14, 1246–1249, doi:10.1029/GL014i012p01246, 1987.
- 22
- 23 Dacey, J. W. H. and Wakeham, S. G.: Oceanic dimethylsulfide: production during zooplankton grazing on phytoplankton,  
24 *Science*, 233, 1314–1316, doi: 10.1126/science.233.4770.1314, 1986.
- 25
- 26 Ducklow, H., Dickson, M.-L., Kirchman, D., Steward, G., Orchardo, J., Marra, J., and Azam, F.: Constraining bacterial  
27 production, conversion efficiency and respiration in the Ross Sea, Antarctica, January-February 1997. *Deep-Sea Res. II*, 47,  
28 3227-3247, doi: 10.1016/S0967-0645(00)00066-7, 2000.
- 29
- 30 Franklin, D. J., Poulton, A. J., Steinke, M., Young, J., Peeken, I., and Malin, G.: Dimethylsulphide, DMSP-lyase activity and  
31 microplankton community structure inside and outside of the Mauritanian upwelling, *Prog. Oceanogr.*, 83, 134–142,  
32 doi:10.1016/j.pocean.2009.07.011, 2009.
- 33 Frouin, R., Franz, B. and Wang, M.: Algorithm to estimate PAR from SeaWiFS data Version 1.2-Documentation., 2003.

- 1 Gabric, A. J., Matrai, P. A., and Vernet, M.: Modelling the production and cycling of dimethylsulphide during the vernal bloom  
2 in the Barents Sea, *Tellus*, 51B, 919-937, doi: /10.3402/tellusb.v51i5.16505, 1999.
- 3 Galí, M. and Simó, R.: A meta-analysis of oceanic DMS and DMSP cycling processes: Disentangling the summer paradox,  
4 *Global Biogeochem. Cycles*, 29, 496–515, doi:10.1002/2014GB004940, 2015.
- 5 Galí, M., Devred, E., Levasseur, M., Royer, S.-J., and Babin, M.: A remote sensing algorithm for planktonic  
6 dimethylsulfoniopropionate (DMSP) and an analysis of global patterns, *Remote Sens. Environ.*, 171, 171–184,  
7 doi:10.1016/j.rse.2015.10.012, 2015.
- 8 Galí, M., Levasseur, M., Devred, E., Simó, R., and Babin, M.: Sea-surface dimethylsulfide (DMS) concentration from satellite  
9 data at global and regional scales, *Biogeosciences*, 15, 3497–3519, doi:10.5194/bg-2018-18, 2018.
- 10
- 11 Goes, J., Saino, T., Oaku, H., Ishizaka, J., Wong, C., and Nojiri, Y: Basin scale estimates of sea surface nitrate and new  
12 production from remotely sensed sea surface temperature and chlorophyll, *Geophys. Res. Lett.*, 27, 1263–1266,  
13 doi:10.1029/1999GL002353, 2000.
- 14
- 15 Gordon, H. R., Boynton, G. C., Balch, W. M., Groom, S. B., Harbour, D. S., and Smyth, T. J.: Retrieval of coccolithophore  
16 calcite concentration from SeaWiFS imagery, *Geophys. Res. Lett.*, 28, 1587–1590, doi:10.1029/2000GL012025, 2001.
- 17
- 18 Gregr, E., and Bodtker, K.: Adaptive classification of marine ecosystems: Identifying biologically meaningful regions in the  
19 marine environment, *Deep-Sea Res. Pt. I*, 54, 385–402, doi:10.1016/j.dsr.2006.11.004, 2007.
- 20
- 21 Harada, H., Vila-Costa, M., Cebrian, J., and Kiene, R.: Effects of UV radiation and nitrate limitation on the production of  
22 biogenic sulfur compounds by marine phytoplankton, *Aquat. Bot.*, 90, 37–42, doi:10.1016/j.aquabot.2008.05.004, 2009.
- 23
- 24 Hatton, A. D., Turner, S. M., Malin, G., and Liss, P. S.: Dimethylsulphoxide and other biogenic sulphur compounds in the  
25 Galapagos Plume, *Deep-Sea Res. Pt. II*, 45, 1043–1053, doi:10.1016/S0967-0645(98)00017-4, 1998.
- 26
- 27 Hatton, A. D. Malin G., and Liss, P.S., Distribution of biogenic sulphur compounds during and just after the southwest  
28 monsoon in the Arabian Sea, *Dee-Sea Res. Pt. II*, 46, 617–632, doi:10.1016/S0967-0645(98)00120-9, 1999.
- 29
- 30 Hayashida, H., Steiner, N., Monohan, A., Galindo, V., Lizotte, M., and Levasseur, M.: Implications of sea-ice biogeochemistry  
31 for oceanic production and emissions of dimethyl sulfide in the Arctic, *Biogeosciences*, 14, 3129–3155, 2017.

1  
2 Hill, R. W., White, B. A., Cottrell, M. T., and Dacey, J. W. H.: Virus-mediated total release of dimethylsulfoniopropionate  
3 from marine phytoplankton: a potential climate process, *Aquat. Microb. Ecol.*, 14: 1–6, doi: 10.3354/ame014001, 1998.  
4  
5 Hind, A. J., Rauschenberg, C. D., Johnson, J. E., Yang, M., Matrai, P. A.: The use of algorithms to predict surface seawater  
6 dimethyl sulphide concentrations in the SE Pacific, a region of steep gradients in primary productivity, biomass and mixed  
7 layer depth, *Biogeosciences*, 8, 1–16, doi:10.5194/bg-8-1-2011, 2011.  
8  
9 Hirata, T., Aiken, J., Hardman-Mountford, N., Smyth, T. J., and Barlow, R. G.: An absorption model to determine  
10 phytoplankton size classes from satellite ocean colour, *Remote Sens. Environ.*, 112, 3153–3159,  
11 doi:10.1016/j.rse.2008.03.011, 2008.  
12  
13 Hirata, T., Hardman-Mountford, N. J., Brewin, R. J., Aiken, J., Barlow, R., Suzuki, K., Isada, T., Howell, E., Hashioka, T.,  
14 Noguchi-Aita, M., and Yamanaka, Y.: Synoptic relationships between surface Chlorophyll-a and diagnostic pigments specific  
15 to phytoplankton functional types, *Biogeosciences*, 8, 311–327, doi:10.5194/bg-8-311-2011, 2011.  
16  
17 Hockin, N. L., Mock, T., Mulholland, F., Kopriva, S., and Malin, G.: The response of diatom central carbon metabolism to  
18 nitrogen starvation is different from that of green algae and higher plants, *Plant Physiol.*, 158, 299–312,  
19 doi:10.1104/pp.111.184333, 2012.  
20  
21 Holligan, P. M., Turner, S. M., and Liss, P. S.: Measurements of dimethyl sulphide in frontal regions, *Cont. Shelf Res.*, 7, 213-  
22 224, doi: 10.1016/0278-4343(87)90080-X, 1987.  
23  
24 Hu, C., Lee, Z. and Franz, B.: Chlorophyll *a* algorithms for oligotrophic oceans: A novel approach based on three-band  
reflectance difference, *J. Geophys. Res.*, 117(C1), C01011, doi:10.1029/2011JC007395, 2012.  
25  
26 Izett, R. W., Manning, C. C., Hamme, R. C., and Tortell, P. D.: Refined Estimates of Net Community Production in the  
Subarctic Northeast Pacific Derived From  $\Delta O_2/Ar$  Measurements With  $N_2O$ -Based Corrections for Vertical Mixing, *Global*  
27 *Biogeochem. Cy.*, 32, 326–350, doi:10.1002/2017GB005792, 2018.  
28  
29 Jarníková, T., Dacey, J., Lizotte, M., Levasseur, M., and Tortell, P.: The distribution of methylated sulfur compounds, DMS  
30 and DMSP, in Canadian subarctic and Arctic marine waters during summer 2015, *Biogeosciences*, 15, 2449–2465,  
31 doi:10.5194/bg-15-2449-2018, 2018.  
32

1 Jarníková, T., and Tortell, P. D.: Towards a revised climatology of summertime dimethylsulfide concentrations and sea–air  
2 fluxes in the Southern Ocean, *Environ. Chem.*, 13, 364–378, doi:10.1071/EN14272, 2016.

3

4 Johnson, K., Miller, L., Sutherland, N., and Wong, C. S.: Iron transport by mesoscale Haida eddies in the Gulf of Alaska,  
5 *Deep-Sea Res. Pt. II*, 52, 933–953, doi:10.1016/j.dsr2.2004.08.017, 2005.

6

7 Johnson, W., Soule, M., and Kujawinski, E.: Evidence for quorum sensing and differential metabolite production by a marine  
8 bacterium in response to DMSP, *ISME J.*, 10, 2304–2316, doi:10.1038/ismej.2016.6, 2016.

9

10 Kaiser, J., Reuer, M. K., Barnett, B., and Bender, M. L.: Marine productivity estimates from continuous O<sub>2</sub>/Ar ratio  
11 measurements by membrane inlet mass spectrometry, *Geophys. Res. Lett.*, 32, L19605, doi:10.1029/2005GL023459, 2005.

12

13 Keller, M. D.: Dimethyl Sulfide Production and Marine Phytoplankton: The Importance of Species Composition and Cell Size,  
14 *Biol. Oceanogr.*, 6, 375–382, doi:10.1080/01965581.1988.10749540, 1989.

15

16 Kettle, A. J., Andreae, M. O., Amouroux, D., Andreae, T. W., Bates, T. S., Berresheim, H., Bingemer, H., Boniforti, R., Curran,  
17 M. A., DiTullio, G. R., Helas, G., Jones, G. B., Keller, M. D., Kiene, R. P., Leck, C., Lefebvre, M., Malin, G., Maspero, M.,  
18 Matrai, P., McTaggart, A. R., Mihalopoulos, N., Nguyen, B. C., Novo, A., Putaud, J. P., Rapsomanikis, S., Roberts, G.,  
19 Schebeske, G., Sharma, S., Simó, R., Staubes, R., Turner, S., and Uher, G.: A global database of sea surface dimethylsulfide  
20 (DMS) measurements and a procedure to predict sea surface DMS as a function of latitude, longitude, and month, *Global*  
21 *Biogeochem. Cy.*, 13, 399–444, doi:10.1029/1999GB900004, 1999.

22

23 Kiene, R. P., and Linn, L. J.: Distribution and turnover of dissolved DMSP and its relationship with bacterial production and  
24 dimethylsulfide in the Gulf of Mexico, *Limnol. Oceanogr.*, 45, 849–861, doi:10.4319/lo.2000.45.4.0849, 2000.

25

26 Kiene, R.P., and Service, S.: Decomposition of dissolved DMSP and DMS in estuarine waters: dependence on temperature  
27 and substrate concentration., *Mar. Ecol. Prog. Ser.*, 76, 1–11, doi:10.3354/meps076001, 1991.

28

29 Kiene, R. P., and Slezak, D.: Low dissolved DMSP concentrations in seawater revealed by small-volume gravity filtration and  
30 dialysis sampling, *Limnol. Oceanogr.-Meth.*, 4, 80–95, doi:10.4319/lom.2006.4.80, 2006.

31

32 Kiene, R. P., Linn, L. J., and Bruton, J. A.: New and important roles for DMSP in marine microbial communities, *J. Sea. Res.*,  
33 43, 209–224, doi:10.1016/S1385-1101(00)00023-X, 2000.

- 1 Kiene, R. P., Kieber, D. J., Slezak, D., Toole, D. A., Valle, D. del, Bisgrove, J., Brinkley, J. and Rellinger, A.: Distribution  
2 and cycling of dimethylsulfide, dimethylsulfoniopropionate, and dimethylsulfoxide during spring and early summer in the  
3 Southern Ocean south of New Zealand, *Aquat. Sci.*, 69, 305–319, doi:10.1007/s00027-007-0892-3, 2007.
- 4 Kinsey, J. D., Kieber, D. J., Neale, P. J.: Effects of iron limitation and UV radiation on *Phaeocystis antarctic* growth and  
5 dimethylsulfoniopropionate, dimethylsulfoxide and acrylate concentrations, *Environ. Chem.*, 13, 195–211,  
6 doi:10.1071/EN14275, 2016.
- 7 Lam, P. J., and Letters, J.K.: The continental margin is a key source of iron to the HNLC North Pacific Ocean, *Geophys. Res.*  
8 *Let.*, 35, L07608, doi:10.1029/2008GL033294, 2008.
- 9
- 10 Lana, A., Bell, T. G., Simó, R., Vallina, S. M., Ballabrera-Poy, J., Kettle, A. J., Dachs, J., Bopp, L., Saltzman, E. S., Stefels,  
11 J., Johnson, J. E., and Liss, P. S.: An updated climatology of surface dimethylsulfide concentrations and emission fluxes in  
12 the global ocean, *Global Biogeochem. Cy.*, 25, GB1004, doi:10.1029/2010GB003850, 2011.
- 13
- 14 Levasseur, M., Gosselin, M., Michaud, S.: A new source of dimethylsulfide (DMS) for the arctic atmosphere: ice diatoms,  
15 *Mar. Biol.*, 121, 381–387, doi:10.1007/BF00346748, 1994.
- 16
- 17 Levasseur, M., Michaud, S., Egge, J., Cantin, G., Nejstgaard, J. C., Sanders, R., Fernandez, E., Solberg, P. T., Heimdal, B.,  
18 and Gosselin, M.: Production of DMSP and DMS during a mesocosm study of an *Emiliana huxleyi* bloom: influence of  
19 bacteria and *Calanus finmarchicus* grazing, *Mar. Biol.*, 126, 609–618, doi:10.1007/BF00351328, 1996.
- 20
- 21 Levasseur, M., Scarratt, M. G., Michaud, S., Merzouk, A., Wong, C., Arychuk, M., Richardson, W., Rivkin, R. B., Hale, M.,  
22 Wong, E., Marchetti, A., and Kiyosawa, H.: DMSP and DMS dynamics during a mesoscale iron fertilization experiment in  
23 the Northeast Pacific—Part I: Temporal and vertical distributions, *Deep-Sea Res.*, Pt. II 53, 2353–2369,  
24 doi:10.1016/j.dsr2.2006.05.023, 2006.
- 25
- 26 Levine, N. M., Toole, D. A., Neeley, A., Bates, N. R., Doney, S. C., Dacey, J. W. H.: Revising upper-ocean sulfur dynamics  
27 near Bermuda: new lessons from 3 years of concentration and rate measurements, *Environ. Chem.*, 13, 302–313,  
28 doi:10.1071/EN15045, 2016.
- 29
- 30 Li, H., Liu, Z., Xu, J., Wu, X., Chaohui, S., Lu, S., and Minjie, C.: Manual of Global Ocean Argo gridded data set (BOA-  
31 Argo) (Version 2017), 2017.
- 32

- 1 Locarnini, S., Turner, S. and Liss, P.: The distribution of dimethylsulfide, DMS, and dimethylsulfoniopropionate, DMSP, in  
2 waters off the Western Coast of Ireland, *Cont. Shelf Res.*, 18, 1455–1473, doi:10.1016/S0278-4343(98)00035-1, 1998.  
3
- 4 Longhurst, A. R.: *Ecological Geography of the Sea*, 2nd ed. Elsevier, doi:10.1016/B978-0-12-455521-1.X5000-1, 2007.  
5
- 6 Lovelock, J., Maggs, R., and Rasmussen, R.: Atmospheric dimethyl sulphide and the natural sulphur cycle, *Nature*, 237, 452–  
7 453, doi:10.1038/237452a0. 1972.  
8
- 9 Malin, G., Turner, S., Liss, P., Holligan, P., and Harbour, D.: Dimethylsulphide and dimethylsulphoniopropionate in the  
10 Northeast Atlantic during the summer coccolithophore bloom, *Deep-Sea Res. Pt. I*, 40, 1487–1508, doi:10.1016/0967-  
11 0637(93)90125-M, 1993.  
12
- 13 Matrai, P. A. and Keller, M. D.: Dimethylsulfide in a large-scale coccolithophore bloom in the Gulf of Maine, *Cont. Shelf*  
14 *Res.*, 13, 831–843, doi:10.1016/0278-4343(93)90012-M, 1993.  
15
- 16 Matrai, P. A., and Vernet, M.: Dynamics of the vernal bloom in the marginal sea ice zone of the Barents Sea: Dimethyl sulphide  
17 and dimethylsulfoniopropionate budgets, *J. Geophys. Res.*, 102, 22965–22979, doi: 10.1029/96JC03870, 1997.  
18
- 19 McParland, E. L. and Levine, N. M.: The role of differential DMSP regulation and community composition in predicting  
20 variability of global surface DMSP concentrations, *Limnol. Oceanogr.*, doi:10.1002/lno.11076, 2018.  
21
- 22 Merzouk, A., Levasseur, M., Scarratt, M. G., Michaud, S., Rivkin, R. B., Hale, M. S., Kiene, R. P., Price, N. M., and Li, W.:  
23 DMSP and DMS dynamics during a mesoscale iron fertilization experiment in the Northeast Pacific–Part II: Biological  
24 cycling, *Deep-Sea Res. Pt. II*, 53, 2370–2383, doi:10.1016/j.dsr2.2006.05.022, 2006.  
25
- 26 Nemcek, N., Ianson, D., and Tortell, P.: A high-resolution survey of DMS, CO<sub>2</sub>, and O<sub>2</sub>/Ar distributions in productive coastal  
27 waters, *Global Biogeochem. Cy.*, 22, GB2009, doi:10.1029/2006GB002879, 2008.
- 28 O’Reilly, J. E., Maritorena, S., Mitchell, B. G., Siegel, D. A., Carder, K. L., Garver, S. A., Kahru, M. and McClain, C.: Ocean  
29 color chlorophyll algorithms for SeaWiFS, *J. Geophys. Res.*, 103(C11), 24937–24953, doi:10.1029/98JC02160, 1998.
- 30 Reisch, C. R., Stoudemayer, M. J., Varaljay, V. A., Amster, I. J., Moran, M. A., and Whitman, W.: Novel pathway for  
31 assimilation of dimethylsulphoniopropionate widespread in marine bacteria, *Nature*, 473, 208–211, doi:10.1038/nature10078,  
32 2011.



1  
2 Reuer, M., Barnett, B., Bender, M., Falkowski, P., and Hendricks, M.: New estimates of Southern Ocean biological production  
3 rates from O<sub>2</sub>/Ar ratios and the triple isotope composition of O<sub>2</sub>, *Deep-Sea Res. Pt. I*, 54, 951–974,  
4 doi:10.1016/j.dsr.2007.02.007, 2007.  
5  
6 Reygondeau, G., Longhurst, A., Martinez, E., Beaugrand, G., Antoine, D., and Maury, O.: Dynamic biogeochemical provinces  
7 in the global ocean, *Global Biogeochem. Cy.*, 27, 1046–1058, doi:10.1002/gbc.20089, 2013.  
8  
9 Ribalet, F., Marchetti, A., Hubbard, K., Brown, K., Durkin, C., Morales, R., Robert, M., Swalwell, J., Tortell, P., and Armbrust,  
10 V.: Unveiling a phytoplankton hotspot at a narrow boundary between coastal and offshore waters, *P. Natl. A. Sci. USA*, 107,  
11 16571–16576, doi:10.1073/pnas.1005638107, 2010.  
12  
13 Roesler, C., and Barnard, A.: Optical proxy for phytoplankton biomass in the absence of photophysiology: Rethinking the  
14 absorption line height, *Methods in Oceanography*, 7, 79–94, doi:10.1016/j.mio.2013.12.003, 2013.  
15  
16 Royer, S.-J., Levasseur, M., Lizotte, M., Arychuk, M., Scarratt, M., Wong, C., Lovejoy, C., Robert, M., Johnson, K., Peña, A.,  
17 Michaud, S., and Kiene, R.: Microbial dimethylsulfoniopropionate (DMSP) dynamics along a natural iron gradient in the  
18 northeast subarctic Pacific, *Limnol. Oceanogr.*, 55, 1614–1626, doi:10.4319/lo.2010.55.4.1614, 2010.  
19  
20 Royer, S. -J., Mahajan, A. S., Gali, M, Saltzman, E., and Simó, R: Small-scale variability patterns of DMS and phytoplankton  
21 in surface waters of the tropical and subtropical Atlantic, Indian and Pacific Oceans, *Geophys. Res. Let.*, 42, 475–483,  
22 doi:10.1002/2014GL062543, 2015.  
23  
24 Saltzman, E. S., King, D. B., Holmen, K., and Leck, C.: Experimental determination of the diffusion coefficient of  
25 dimethylsulfide in water, *J. Geophys. Res.*, 98, 16481–16468, doi:10.1029/93JC01858, 1993.  
26  
27 Saraceno, M., Strub, P. T., and Kosro, P. M.: Estimates of sea surface height and near-surface alongshore coastal currents from  
28 combinations of altimeters and tide gauges, *J. Geophys. Res.-Oceans*, 113, C11013, doi:10.1029/2008JC004756, 2008.  
29  
30 Schuback, N., Schallenberg, C., Duckham, C., Maldonado, M. and Tortell, P.: Interacting Effects of Light and Iron Availability  
31 on the Coupling of Photosynthetic Electron Transport and CO<sub>2</sub>-Assimilation in Marine Phytoplankton, *Plos One*, 10:  
32 e0133235, doi:10.1371/journal.pone.0133235, 2015.  
33

- 1 Seymour, J. R., Simó, R., Ahmed, T., and Stocker, R.: Chemoattraction to Dimethylsulfoniopropionate Throughout the Marine  
2 Microbial Food Web, *Science*, 329, 342–345, doi:10.1126/science.1188418, 2010.
- 3
- 4 Simó, R.: From cells to globe: approaching the dynamics of DMS (P) in the ocean at multiple scales, *Can. J. Fish. Aquat. Sci.*,  
5 61, 673–684, doi:10.1139/f04-030, 2004.
- 6
- 7 Simó, R., and Dachs, J.: Global ocean emission of dimethylsulfide predicted from biogeophysical data, *Global Biogeochem.*  
8 *Cy.*, 16, 1078, doi:10.1029/2001GB001829, 2002.
- 9 Simó, R., Saló, V., Almeda, R., Movilla, J., Trepát, I., Saiz, E. and Calbet, A.: The quantitative role of microzooplankton  
10 grazing in dimethylsulfide (DMS) production in the NW Mediterranean, *Biogeochemistry*, 2, 1–18, doi:10.1007/s10533-018-  
11 0506-2, 2018.
- 12 Simon, M., and Azam, F.: Protein content and protein synthesis rates of planktonic marine bacteria. *Mar. Ecol. Prog. Ser.*, 51,  
13 201-213, doi: 10.3354/meps051201, 1989.
- 14
- 15 Smith, D., and Azam, F.: A simple, economical method for measuring bacterial protein synthesis rates in seawater using <sup>3</sup>H-  
16 leucine, *Marine Microbial Food Webs*, 6, 107–114, 1992.
- 17
- 18 Smith, R. L.: A description of current, wind, and sea level variations during coastal upwelling off the Oregon coast, July–  
19 August 1972, *J. Geophys. Res.*, 79, doi:10.1029/JC079i003p00435, 1974.
- 20
- 21 Stefels, J., van Boekel, W. H. M., Production of DMS from dissolved DMSP in axenic cultures of the marine phytoplankton  
22 species *Phaeocystis* sp. *Mar. Ecol. Prog. Ser.*, 97, 11–18, doi:10.3354/meps097011, 1993.
- 23
- 24 Stefels, J., Steinke, M., Turner, S., Malin, G., and Belviso, S.: Environmental constraints on the production and removal of the  
25 climatically active gas dimethylsulphide (DMS) and implications for ecosystem modelling, *Biogeochemistry*, 83, 245–275,  
26 doi:10.1007/s10533-007-9091-5, 2007.
- 27
- 28 Steiner, N., Robert, M., Arychuk, M., Levasseur, M., Merzouk, A., Peña, A., Richardson, W. and Tortell, P.: Evaluating DMS  
29 measurements and model results in the Northeast subarctic Pacific from 1996–2010, *Biogeochemistry*, 110, 269–285,  
30 doi:10.1007/s10533-011-9669-9, 2012.
- 31

- 1 Steinke, M., Malin, G., Archer, S. D., Burkill, P. H., and Liss, P. S.: DMS production in a coccolithophorid bloom: evidence  
2 for the importance of dinoflagellate DMSP lyases, *Aquat. Microb. Ecol.*, 26, 259–270, doi:10.3354/ame026259, 2002.  
3
- 4 Strub, T., and James, C.: The large-scale summer circulation of the California Current, *Geophys. Res. Lett.*, 22, 207–210,  
5 doi:10.1029/94GL03011, 1995.  
6
- 7 Sunda, W., Kieber, D. J., Kiene, R. P., and Huntsman, S.: An antioxidant function for DMSP and DMS in marine algae, *Nature*,  
8 418, 317–320, doi:10.1038/nature00851, 2002.  
9
- 10 Sunda, W., Hardison, R., Kiene, R., and Bucciarelli, E.: The effect of nitrogen limitation on cellular DMSP and DMS release  
11 in marine phytoplankton: climate feedback implications, *Aquat. Sci.*, 69, 341–351, doi:10.1007/s00027-007-0887-0, 2007.  
12
- 13 Suzuki, K., Minami, C., Liu, H., and Saino, T.: Temporal and spatial patterns of chemotaxonomic algal pigments in the  
14 subarctic Pacific and the Bering Sea during the early summer of 1999, *Deep-Sea Res. Part II*, 49, 5685–5704,  
15 doi:10.1016/s0967-0645(02)00218-7, 2002.  
16
- 17 Sweeney, C., Gloor, E., Jacobson, A. R., Key, R. M., McKinley, G., Sarmiento, J. L., and Wanninkhof, R.: Constraining global  
18 air-sea gas exchange for CO<sub>2</sub> with recent bomb <sup>14</sup>C measurements, *Global Biogeochem. Cy.*, 21, GB2015,  
19 doi:10.1029/2006gb002784, 2007.  
20
- 21 Tabata, S., Thomas, B. and Ramsden, D.: Annual and interannual variability of steric sea level along line P in the northeast  
22 Pacific Ocean, *J. Phys. Oceanogr.*, 16, 1378–1398, doi:10.1175/1520-0485(1986)016<1378:AAIVOS>2.0.CO, 1986.  
23
- 24 Tortell, P. D.: Dissolved gas measurements in oceanic waters made by membrane inlet mass spectrometry, *Limnol. Oceanogr.*-  
25 *Meth.*, 3, 24–37, doi:10.4319/lom.2005.3.24, 2005a.  
26
- 27 Tortell, P. D.: Small-scale heterogeneity of dissolved gas concentrations in marine continental shelf waters, *Geochem. Geophys.*  
28 *Geosy.*, 6, Q11M04, doi:10.1029/2005GC000953, 2005b.  
29
- 30 Tortell, P. D., Merzouk, A., Ianson, D. Pawlowicz, R., and Yelland, D. R.: Influence of regional climate forcing on surface  
31 water *p*CO<sub>2</sub>, ΔO<sub>2</sub>/Ar and dimethylsulfide (DMS) along the southern British Columbia coast, *Cont. Shelf Res.*, 47, 119–132,  
32 doi:10.1016/j.csr.2012.07.007, 2012.  
33

- 1 Turner, S. M., Nightingale, P. D., Broadgate, W., and Liss, P. S.: The distribution of dimethyl sulphide and  
2 dimethylsulphoniopropionate in Antarctic waters and sea ice, *Deep-Sea Res. Pt. II*, 42, 1059–1080, doi:10.1016/0967-  
3 0645(95)00066-Y, 1995.
- 4
- 5 Uitz, J., Claustre, H., Morel, A., and Hooker, S. B.: Vertical distribution of phytoplankton communities in open ocean: An  
6 assessment based on surface chlorophyll, *J. Geophys. Res.-Oceans*, 111, C08005, doi:10.1029/2005JC003207, 2006.
- 7
- 8 Del Valle, D. A., Kieber, D. J., Toole, D. A., Brinkley, J., and Kiene, R. P.: Biological consumption of dimethylsulfide (DMS)  
9 and its importance in DMS dynamics in the Ross Sea, Antarctica, *Limnol. Oceanogr.*, 54, 785–798,  
10 doi:10.4319/lo.2009.54.3.0785, 2009.
- 11
- 12 Vallina, S., and Simó, R.: Strong relationship between DMS and the solar radiation dose over the global surface ocean, *Science*  
13 315, 506–508, doi:10.1126/science.1133680, 2007.
- 14 Van Heukelem, L., Thomas, C. S.: Computer-assisted high-performance liquid chromatography method development with  
15 applications to the isolation and analysis of phytoplankton pigments, *J. Chromatogr. A* 910, 31–49, doi:10.1016/S0378-  
16 4347(00)00603-4, 2001.
- 17 Venegas, R. M., Strub, P. T., Beier, E., Letelier, R., Thomas, A. C., Cowles, T., James, C., Soto-Mardones, L., and Cabrera,  
18 C.: Satellite-derived variability in chlorophyll, wind stress, sea surface height, and temperature in the northern California  
19 Current System, *J. Geophys. Res.-Oceans* 113, C03015, doi:10.1029/2007JC004481, 2008.
- 20
- 21 Vézina, A.: Ecosystem modelling of the cycling of marine dimethylsulfide: a review of current approaches and of the potential  
22 for extrapolation to global scales, *Can. J. Fish. Aquat. Sci.*, 61, 845–856, doi:10.1139/f04-025, 2004.
- 23
- 24 Vidussi, F., Claustre, H., Manca, B. B., Luchetta, A., and Marty, J.-C.: Phytoplankton pigment distribution in relation to upper  
25 thermocline circulation in the eastern Mediterranean Sea during winter, *J. Geophys. Res.-Oceans*, 106,  
26 doi:10.1029/1999JC000308, 1993–19956, 2001.
- 27
- 28 Vila-Costa, M., Kiene, R., and Simó, R.: Seasonal variability of the dynamics of dimethylated sulfur compounds in a coastal  
29 northwest Mediterranean site, *Limnol. Oceanogr.*, 53, doi:10.4319/lo.2008.53.1.0198, 198–211, 2008.
- 30
- 31 Wang, S., Elliott, S., Maltrud, M., and Cameron-Smith, P.: Influence of explicit *Phaeocystis* parameterizations on the global  
32 distribution of marine dimethyl sulfide, *J. of Geophys. Res.-Biogeo.*, 120, 2158–2177, doi:10.1002/2015JG003017, 2015.

- 1 Watanabe, Y. W., Yoshinari, H., Sakamoto, A., Nakano, Y., Kasamatsu, N., Midorikawa, T. and Ono, T.: Reconstruction of  
2 sea surface dimethylsulfide in the North Pacific during 1970s to 2000s, *Mar. Chem.*, 103, 347–358,  
3 doi:10.1016/j.marchem.2006.10.004, 2007.
- 4 Werdell, J., and Bailey, S.: An improved in-situ bio-optical data set for ocean color algorithm development and satellite data  
5 product validation, *Remote Sens. Environ.*, 98, 122–140, doi:10.1016/j.rse.2005.07.001, 2005.  
6
- 7 Whitney, F. A., Crawford, W. R., and Harrison, P. J.: Physical processes that enhance nutrient transport and primary  
8 productivity in the coastal and open ocean of the subarctic NE Pacific, *Deep-Sea Res. Pt. II*, 52, 681–706,  
9 doi:10.1016/j.dsr2.2004.12.023, 2005.  
10
- 11 Wolfe, G. V., and Kiene, R.P.: Radioisotope and chemical inhibitor measurements of dimethyl sulfide consumption rates and  
12 kinetics in estuarine waters, *Mar. Ecol. Prog. Ser.*, 99, 261–269, doi:10.3354/meps099261, 1993.  
13
- 14 Wolfe, G. V., Strom, S. L., Holmes, J. L., Radzio, T. and Olson, B. M.: Dimethylsulfio-*propionate* cleavage by marine  
15 phytoplankton in response to mechanical, chemical, or dark stress, *J. Phycol.*, 38, 948–960, doi:10.1046/j.1529-8817.2002.t01-  
16 1-01100.x, 2002.  
17
- 18 Wong, C., Wong, S., Richardson, W., Ith, G., Arychuk, M., and Page, J. Temporal and spatial distribution of dimethylsulfide  
19 in the subarctic northeast Pacific Ocean: a high-nutrient–low-chlorophyll region, *Tellus 57B*, 317–331, doi:10.1111/j.1600-  
20 0889.2005.00156.x, 2005.  
21
- 22 Wu, X., Li, P., Liu, C., Zhang, H., Yang, G., Zhang, S., and Zhu, M.: Biogeochemistry of Dimethylsulfide,  
23 Dimethylsulfoniopropionate, and Acrylic Acid in the Changjiang Estuary and the East China Sea, *J. Geophys. Res.-Oceans*,  
24 122, 10,245–10,261, doi:10.1002/2017JC013265, 2017.  
25
- 26 Yoch, D. C.: Dimethylsulfoniopropionate: its sources, role in the marine food web, and biological degradation to  
27 dimethylsulfide, *Appl. Environ. Microbiol.*, 68, 5804–5815, doi:10.1128/AEM.68.12.5804-5815.2002, 2002.  
28
- 29 Zeng, C., Rosengard, S. Z., Burt, W., Peña, A., Nemcek, N., Zeng, T., Arrigo, K. R., and Tortell, P. D.: Optically-derived  
30 estimates of phytoplankton size class and taxonomic group biomass in the Eastern Subarctic Pacific Ocean, *Deep-Sea Res. Pt.*  
31 *I*, 136, 107–118, doi:10.1016/j.dsr.2018.04.001, 2018.  
32
- 33 Zindler, C., Peeken, I., and Marandino, C.: Environmental control on the variability of DMS and DMSP in the Mauritanian  
34 upwelling region, *Biogeosciences*, 9, 1041–1051, doi:10.5194/bg-9-1041-2012, 2012.

1

2 Zubkov, M. V., Fuchs, B. M., Archer, S. D., and Kiene, R. P.: Rapid turnover of dissolved DMS and DMSP by defined  
 3 bacterioplankton communities in the stratified euphotic zone of the North Sea, *Deep-Sea Res. Pt. II*, 49, 3017–3038,  
 4 doi:10.1016/S0967-0645(02)00069-3, 2002.

5 Zubkov, M., Linn, L. J., Amann, R., and Kiene, R. P. Temporal patterns of biological dimethylsulfide (DMS) consumption  
 6 during laboratory-induced phytoplankton bloom cycles, *Mar. Ecol. Prog. Ser.*, 271, 77–86, doi:10.3354/meps271077, 2004.

7

8

9

10

11

12

13

14

15

16 **Table 1. Summary of DMS data included in this study. With the exception of the PMEL data, all measurements are derived from**  
 17 **membrane inlet mass spectrometry (MIMS).**

Cruise abbreviation	Vessel affiliation; cruise name and number	Sampling dates	Areal extent	Provinces included	No. data points	References
VII04	DFO; Central Coast BioChemical Study; 2004-24	12–19 Aug 2004	48° N - 52° N 131 ° W - 123° W	ALSK, CCAL	1913	(Nemcek et al. 2008)
LPJ07	DFO; Line P; 2007-13	1–16 Jun 2007	47° N - 55° N 146 ° W - 123° W	ALSK, CCAL, PSAE	21478	(Asher et al. 2011)
LPA07	DFO; Line P; 2007-15	16–30 Aug 2007	48° N - 54° N 146 ° W - 123° W	ALSK, CCAL, PSAE	16418	(Asher et al. 2011)
LPJ08	DFO; Line P; 2008-26	1–15 Jun 2008	48°N - 52°N 146 ° W - 123° W	ALSK, CCAL, PSAE	15304	(Asher et al. 2011)
LPA08	DFO; Line P; 2008-27	14–30 Aug 2008	48°N - 52°N 146 ° W - 123° W	ALSK, CCAL, PSAE	20881	(Asher et al. 2011)
VII10	DFO; La Perouse; 2010-12	1–4 Jun 2010	48°N - 52°N 130 ° W - 123° W	ALSK, CCAL	4551	(Tortell et al. 2012)

WCAC10	DFO; Ocean Acidification; 2010-36	22 Jul–15 Aug 2010	47°N - 57°N 138 ° W - 123° W	ALSK, CCAL, PSAE	25167	(Asher et al. 2017)
LPA11	DFO; Line P; 2011-27	19–28 Aug 2011	48° N - 51° N 146 ° W - 126° W	CCAL, PSAE	10802	(Asher et al. 2017)
LPA14	DFO; Line P and Strait of Georgia; 2014-19	29–31 Aug 2014	50° N - 51° N 145° W - 134° W	PSAE	2560	(Asher et al. 2015)
O16	UNOLS; Resolving DMS 1: OC-1607A	12–27 Jul 2016	45° N - 56° N 143 ° W - 124° W	ALSK, CCAL, PSAE	18712	Previously unpublished
O17	UNOLS; Resolving DMS II: OC-1708A	12–27 Aug 2017	47° N - 57° N 146 ° W - 126° W	ALSK, CCAL, PSAE	10015	Previously unpublished
PMEL	various	various, 1984–2004	45° N - 61° N 167 ° W - 124° W	ALSK, CCAL, PSAE	3236	Various

1 **Table 2. Summertime DMS data coverage across the NESAP region and within Longhurst provinces. Values indicate the number**  
2 **of data-containing 1° x 1° spatial bins out of the total number of bins within the given area, with percent coverage of area shown in**  
3 **parentheses. The left column represents the coverage for the PMEL data set (as utilized by L11) and the right column represents**  
4 **the updated data set containing both PMEL measurements and MIM-based DMS concentration measurements.**

5

<b>Province Name</b>	<b>PMEL</b>	<b>This Study</b>
<b>CCAL</b>	30/75 (40.0 %)	45/75 (60.0 %)
<b>ALSK</b>	61/119 (51.3 %)	83/119 (69.8 %)
<b>PSAE</b>	5/430 (12.8 %)	114/430 (26.5 %)
<b>Total</b>	126/1140 (11.1 %)	249/1140 (21.8 %)

6

7



1 **Table 3. Mean DMS concentrations, sea-air fluxes and total summertime DMS flux for the PMEL data set utilized by L11, and the**  
 2 **updated data based used in this study.**

3

	<b>PMEL</b>			<b>This Study</b>				
<b>Province</b>	DMS (nM)	DMS	Flux	Total summer DMS	DMS (nM)	DMS	Flux	Total summer DMS
<b>Name</b>		( $\mu\text{mol m}^{-2} \text{d}^{-1}$ )		flux (Tg S)		( $\mu\text{mol m}^{-2} \text{d}^{-1}$ )		flux (Tg S)
<b>CCAL</b>	$4.0 \pm 0.5$	$4.4 \pm 0.95$		0.01	$4.6 \pm 0.4$	$6.3 \pm 0.7$		0.02
<b>ALSK</b>	$8.9 \pm 1.1$	$16.4 \pm 4.0$		0.06	$7.5 \pm 0.9$	$14.4 \pm 3.0$		0.05
<b>PSAE</b>	$8.9 \pm 0.7$	$21.0 \pm 4.0$		0.38	$6.5 \pm 0.4$	$16.5 \pm 2.2$		0.30
<b>Total</b>	$7.2 \pm 0.5$	$12.7 \pm 2.0$		0.32	$6.2 \pm 0.3$	$12.2 \pm 1.4$		0.30

4

5

1 Table 4. Pearson's correlation coefficients between DMS concentrations and other oceanographic variables binned to 1° spatial  
 2 resolution. DMS data were derived from our combined PMEL and MIMS data set, variables derived from in-situ and satellite-  
 3 based data. N represents the number of data pairs available for each correlation calculation. \* indicates significance of  $p < 0.05$ .

Variable	Whole region	CCAL	ALSK	PSAE
Salinity	r = -0.04 N = 223	r = 0.24 N = 31	r = -0.04 N = 83	r = 0.07 N = 102
SST	r = -0.01 N = 248	r = -0.17 N = 44	r = -0.32* N = 83	r = 0.18 N = 114
Chlorophyll- <i>a</i>	r = 0.17* N = 207	r = -0.11 N = 31	r = 0.34* N = 79	r = 0.45* N = 99
Calcite	r = 0.12 N = 205	r = -0.08 N = 30	r = -0.01 N = 83	r = 0.50* N = 99
PAR	r = 0.04 N = 212	r = -0.28 N = 32	r = 0.41* N = 52	r = 0.19 N = 91
Depth	r = -0.05 N = 201	r = 0.20 N = 45	r = -0.34* N = 12	r = -0.02 N = 96
MLD	r = -0.14 N = 98	r = 0.14 N = 21	r = -0.06 N = 11	r = -0.18 N = 70
SSN	r = 0.01 N = 207	r = 0.14 N = 31	r = 0.30* N = 79	r = -0.18 N = 99
SSHA	r = -0.20* N = 207	r = -0.34 N = 30	r = -0.05 N = 80	r = -0.47* N = 102
NCP	r = 0.22* N = 91	r = 0.43* N = 26	r = 0.05 N = 25	r = 0.29 N = 37
Wind	r = 0.17* N = 249	r = -0.06 N = 45	r = 0.08 N = 83	r = 0.29* N = 114

4

5

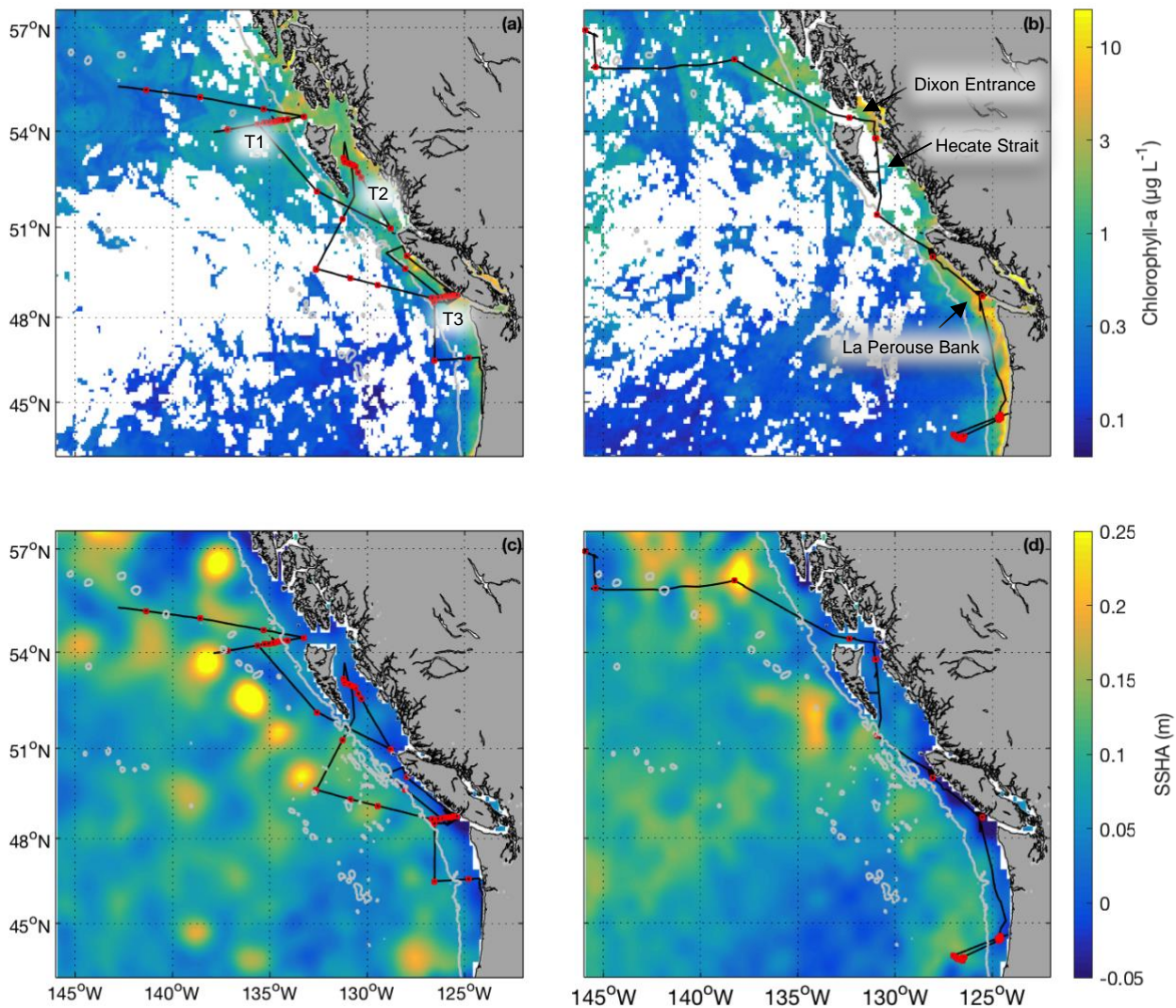
1 **Table 5. Pearson correlation coefficients and root mean square errors (nmol L<sup>-1</sup>) between observed DMS concentrations and empirical predictions derived**  
 2 **from the SD02, VS07 and W07 algorithms, using both published coefficients (original) and coefficients derived specifically for our NESAP observations**  
 3 **using a least-squares approach (custom). Algorithm performance is shown for full NESAP region, as well as the three Longhurst biogeographical**  
 4 **provinces within our study area. \* indicates significance of p<0.05.**

Province	SD02	SD02	VS07	VS07	W07	W07	G18	G18
	original	custom	original	custom	original	custom	original	custom
Whole	r = 0.05	r = 0.08	r = -0.31*	r = 0.31*	r = -0.08	r = 0.17*	r = 0.19	r = 0.26*
region	RMSE = 3.77	RMSE = 3.03	RMSE = 4.95	RMSE = 2.63	RMSE = 67.1	RMSE = 5.86	RMSE = 3.1	RMSE = 19.8
CCAL	r = 0.04	r = 0.62*	r = -0.23	r = 0.23	r = -0.17	r = 0.27	r = 0.72*	r = 0.69*
	RMSE = 3.42	RMSE = 1.61	RMSE = 4.54	RMSE = 1.20	RMSE = 81.6	RMSE = 2.04	RMSE = 1.9	RMSE = 55.2
ALSK	r = 0.16	r = 0.12	r = -0.10	r = 0.10	r = -0.20	r = 0.53*	r = -0.41	r = 0.56
	RMSE = 2.37	RMSE = 2.07	RMSE = 3.43	RMSE = 2.09	RMSE = 47.5	RMSE = 7.19	RMSE = 3.4	RMSE = 31.17
PSAE	r = 0.09	r = 0.23	r = -0.39*	r = 0.39*	r = -0.01	r = 0.44*	r = -0.04	r = 0.26
	RMSE = 3.97	RMSE = 2.94	RMSE = 5.28	RMSE = 2.81	RMSE = 20.6	RMSE = 4.59	RMSE = 3.5	RMSE = 21.3

5

6

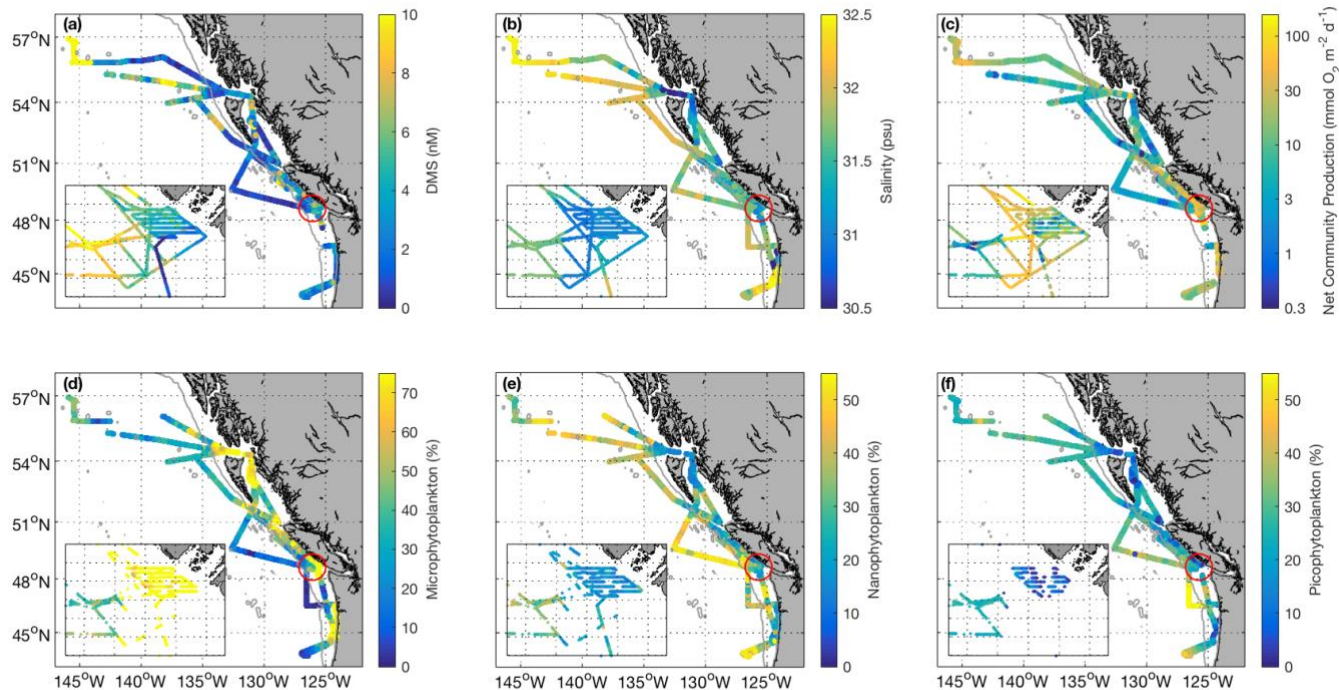
1



2

3 **Figure 1. Cruise tracks and discrete sampling stations (red circles) for the July 2016 (O16) cruise (a,c) and August 2017 (O17) cruise**  
 4 **(b, d). Panels (a) and (b) show chl-*a* concentration (log scale), derived from AquaMODIS satellite, and averaged over the duration**  
 5 **of the respective cruise. Panels (c) and (d) show average sea surface height anomaly (SSHA). Panel (a) shows the location of the T1-**  
 6 **T3 transects surveyed during the 2016, whereas panel (b) shows the geographic location of locations of interest. The grey line**  
 7 **represents the coastal-oceanic boundary, defined here as the 2000 m isobath.**

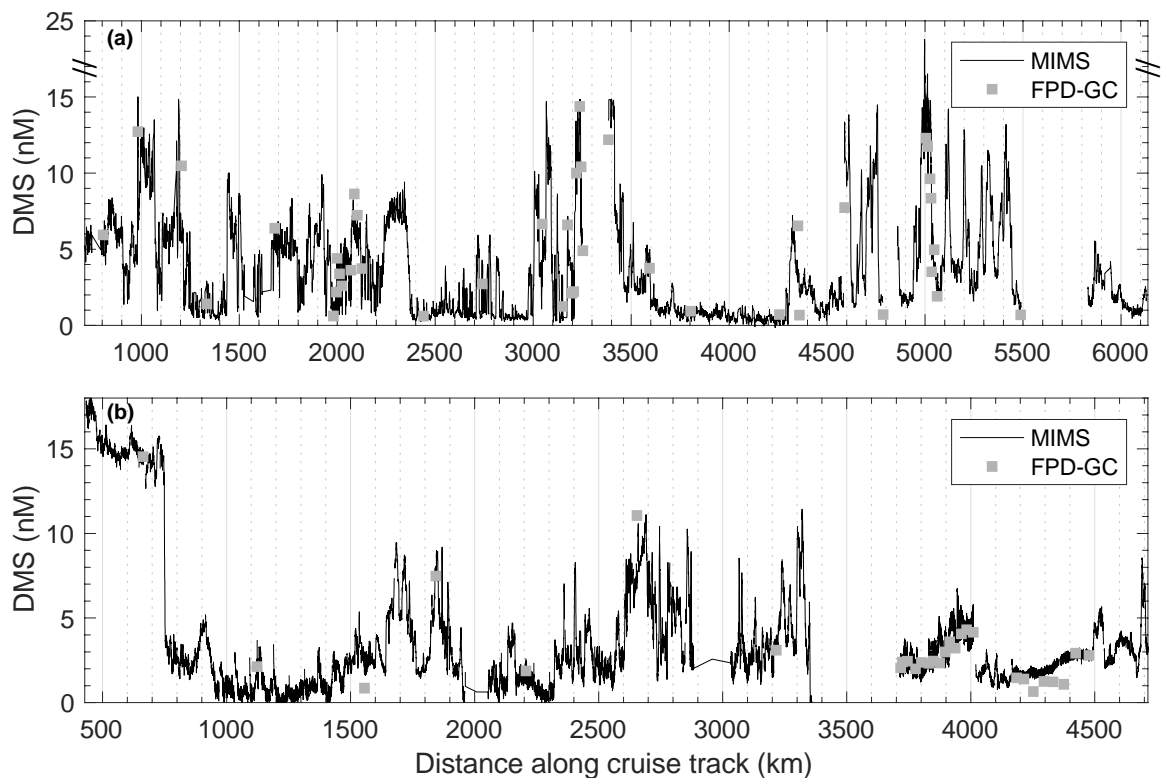
8



1

2 **Figure 2. Spatial distribution of DMS (a), salinity (b), net community production (C; note log scale), and**  
 3 **micro-, nano-, and picophytoplankton relative abundance (d-f) during the O16 cruise July of 2016 and the O17 cruise August of 2017. Colour scaling**  
 4 **on the maps are adjusted to ensure readability and best illustrate spatial patterns. Some data values are higher than the maximum**  
 5 **scale of the colour bar. The inset box shows the La Perouse Bank region, as marked by the red circle. The grey line represents the**  
 6 **coastal-open ocean boundary (2000 m isobath).**

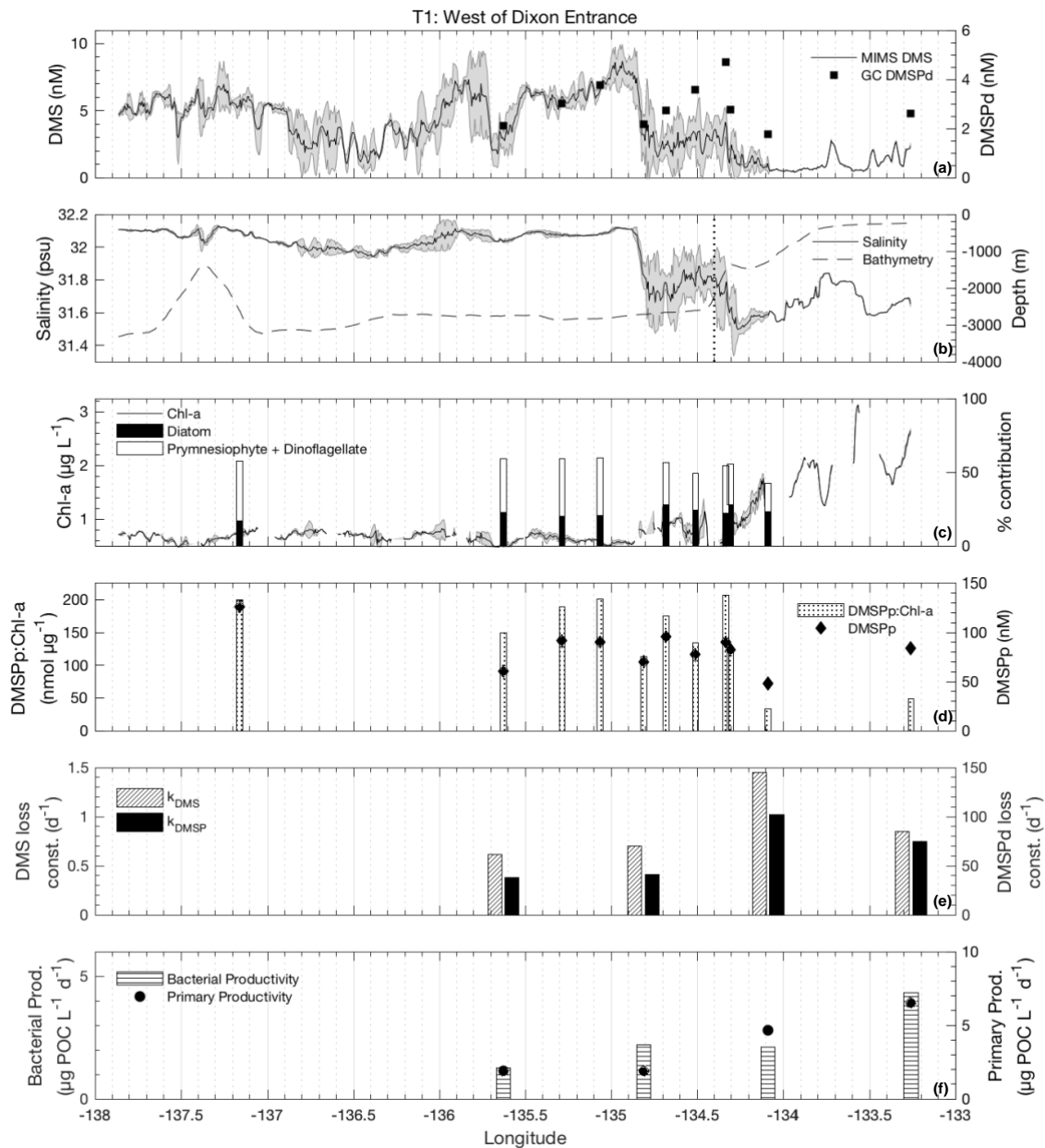
7



1

2 **Figure 3. DMS concentrations during the O16 cruise in July of 2016 (a) and the O17 cruise in August of 2017 (b) as measured by**  
 3 **membrane inlet mass spectrometry (MIMS, continuous black line) and a purge-and-trap sampling system connected to a gas**  
 4 **chromatograph equipped with a flame-photometric detector (grey symbols). Mean absolute error was 0.93 nM and root mean**  
 5 **squared error was 1.4 nM for all paired measurements between the two instruments. A linear regression of the two data sets yields**  
 6 **a coefficients of determination of  $r^2=0.89$ .**

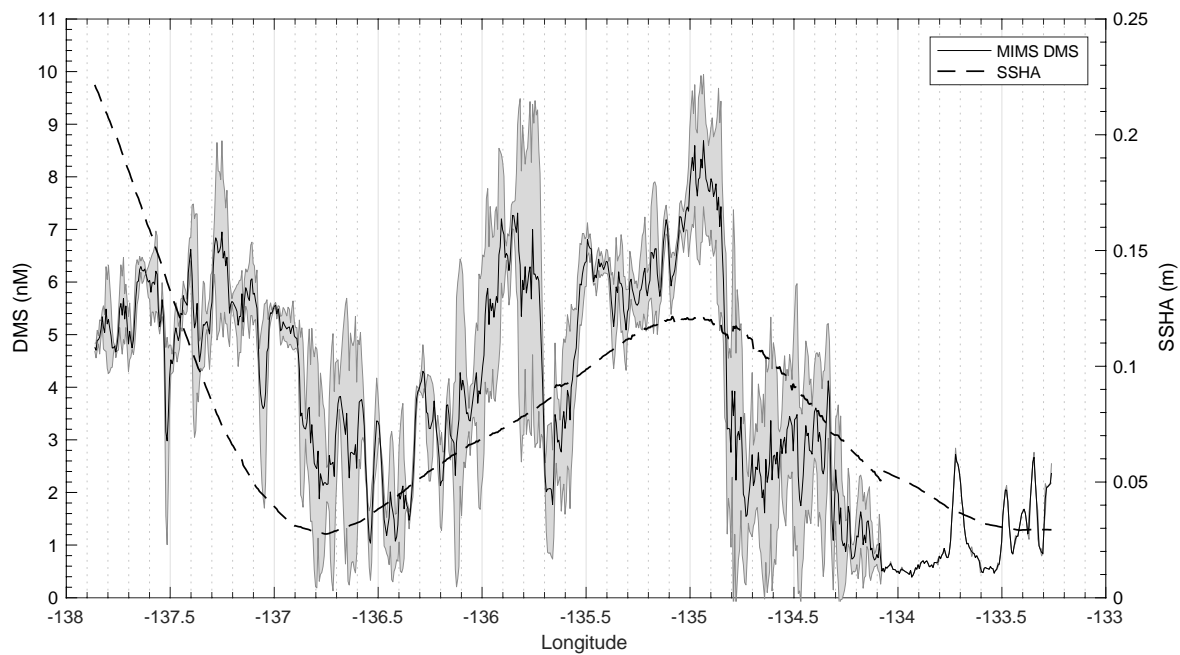
7



1

2 **Figure 4.** MIMS-based DMS concentration measurements and station-based DMSPd measurements (a), salinity and bathymetry  
 3 (b), chl-*a* and HPLC-based station estimates of diatom and prymnesiophyte as defined % contribution to total assemblage (c),  
 4 DMSPp concentrations and DMSPp:chl-*a* ratios (d), DMS/P consumption rate constants (e), and bacterial and primary productivity  
 5 rates (f) along the T1 transect west of Dixon Entrance during July 2016 (O16 cruise). Shaded regions represent standard deviation  
 6 of repeated measurements across the transect. The vertical dotted line in panel (b) indicates the approximate shelf break (2000 m),  
 7 at 134.4° W.

1



2

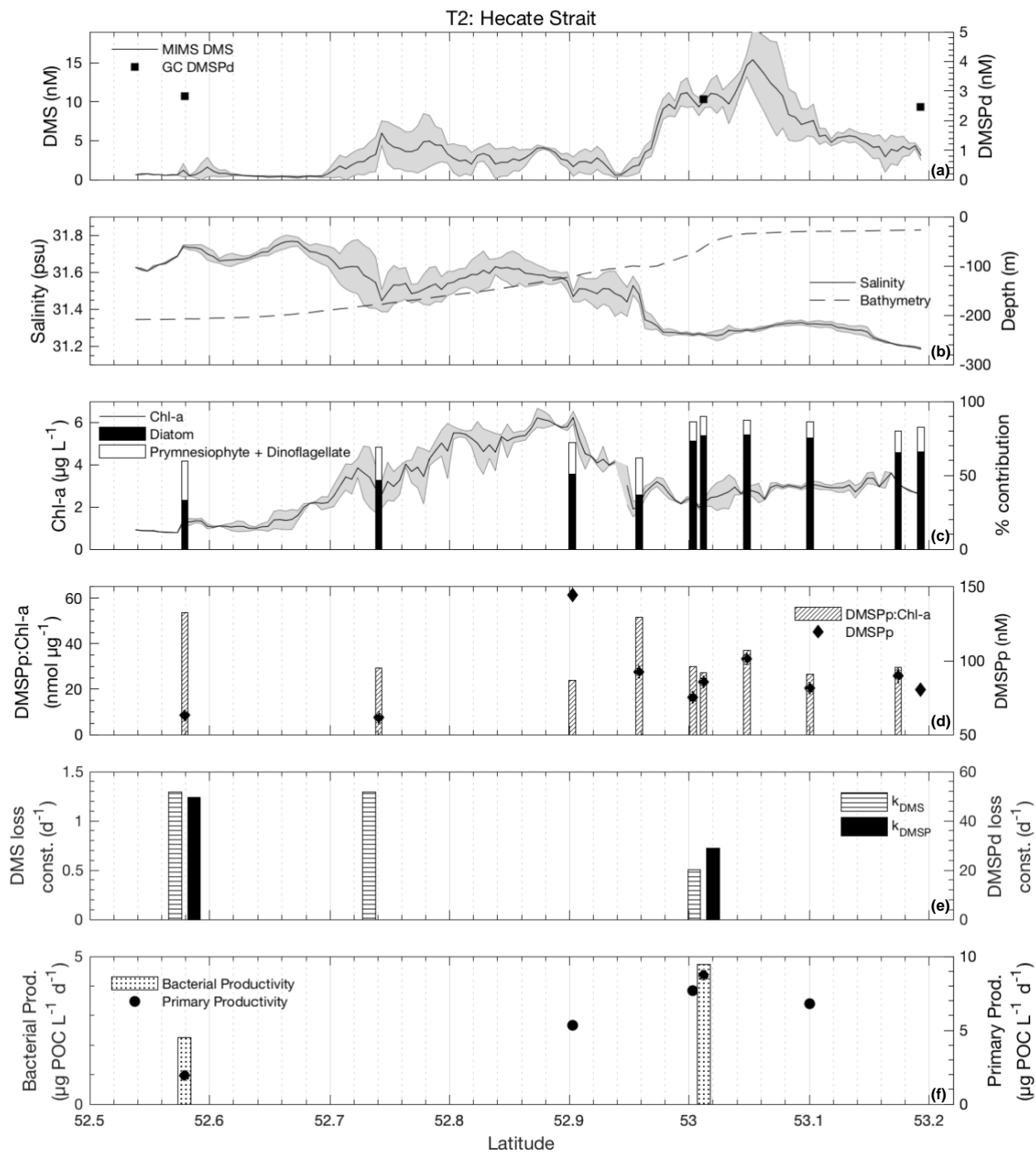
3 **Figure 5. Line plot of sea surface height anomaly (SSHA) on 15 July, 2016 and observed DMS concentrations between 14 July and**  
4 **DMS along the T1 transect is highest in those areas influenced by positive SSHA values.**

5

6

7

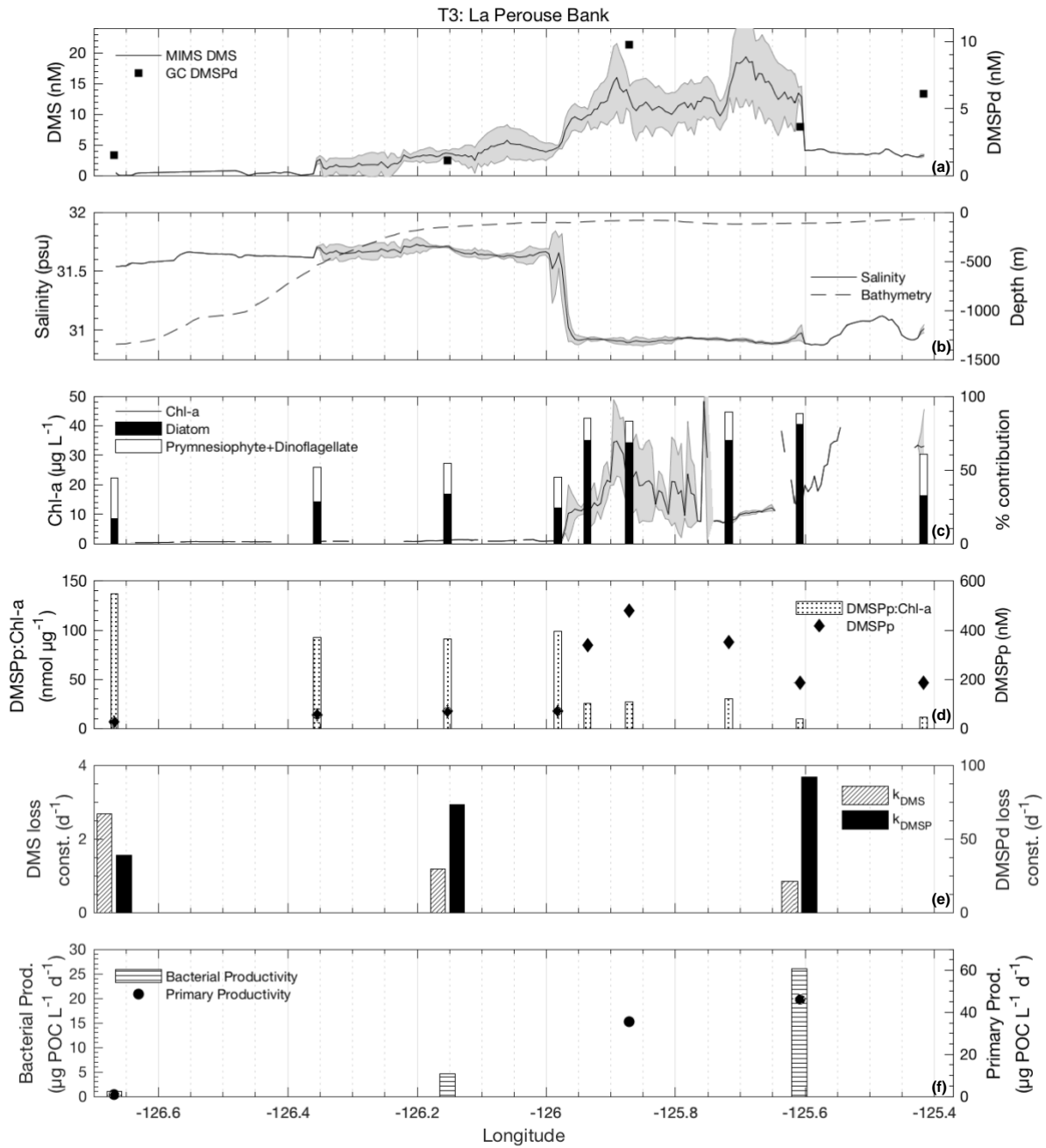




1

2 **Figure 6.** As for Fig. 4, but for the T2 transect.

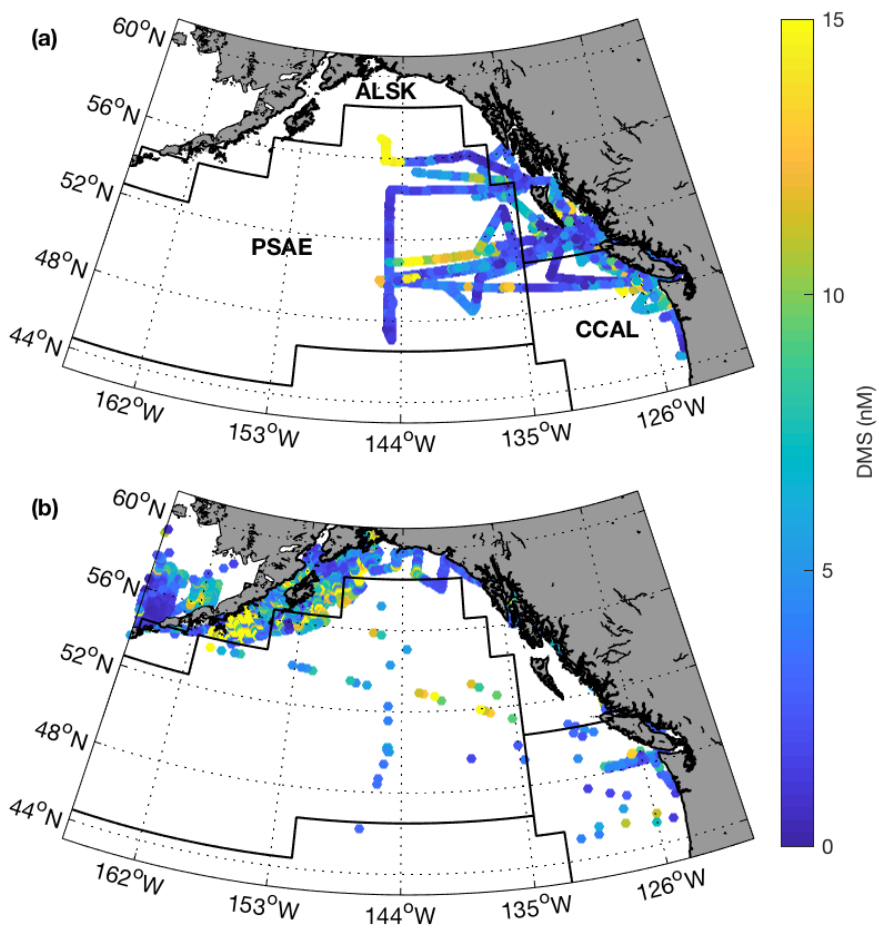
1  
2



3

4 Figure 7. As for Figs. 4 and 6, but for the T3 transect.

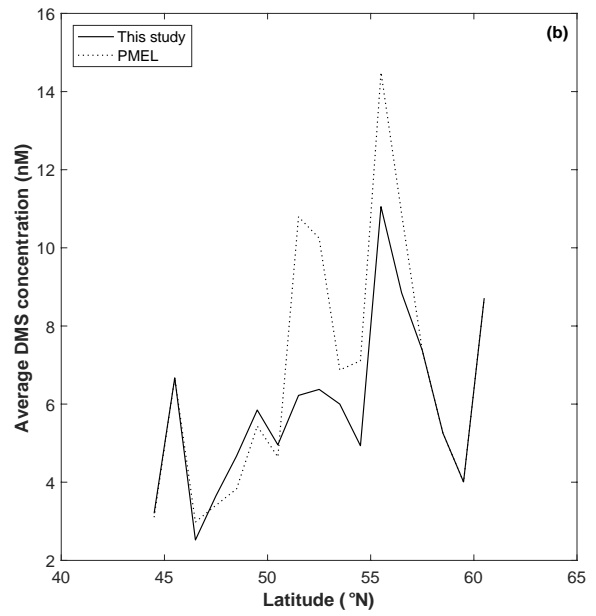
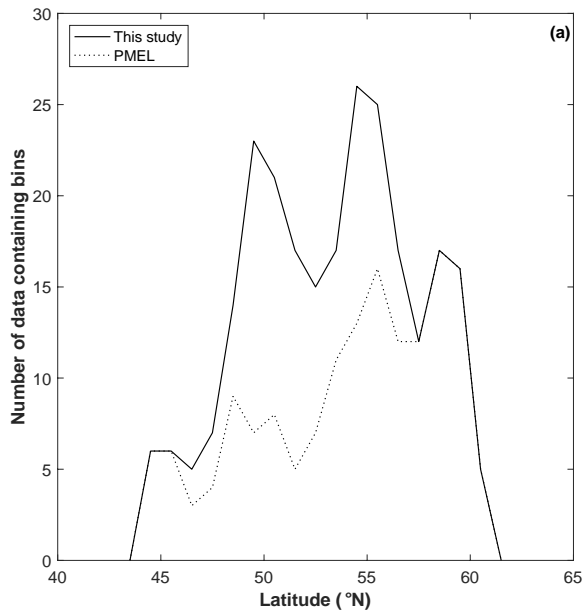
1



2

3 **Figure 8. Spatial distribution of summertime DMS measurements from MIMS (a; 2004-2017) and the PMEL (b; 1984 - 2004) data**  
4 **set. Black lines represent boundaries of Longhurst biogeographical provinces, with province names show in panel (a).**

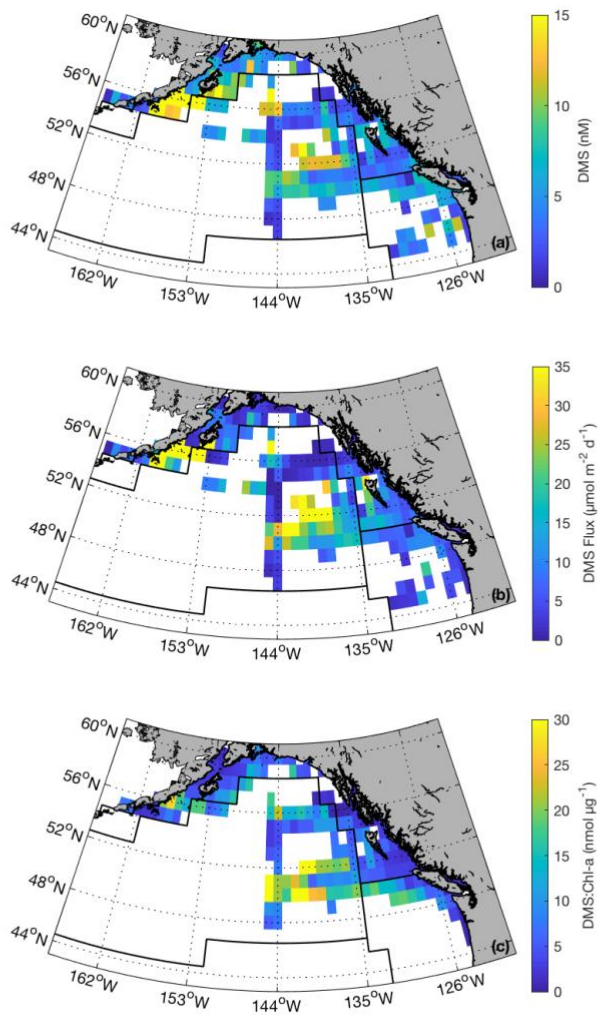
5



1

2 **Figure 9. Latitudinal distribution of data-containing bins (a) and average DMS concentration (b) for PMEL (dotted line) and**  
 3 **combined (PMEL and MIMS) data sets.**

4



1

2 **Figure 10. Summertime DMS concentrations (a), DMS sea-air fluxes (b), and DMS:chl-*a* ratios (c) binned to 1° x 1° spatial**  
 3 **resolution. These maps were derived using our combined PMEL/MIMS data set (1984–2017; June, July and August). Black lines**  
 4 **correspond to boundaries of Longhurst biogeographical provinces (see Fig. 8 for province names). Maximum values (47 nM, 180**  
 5  **$\mu\text{mol m}^{-2} \text{d}^{-1}$ , and 47  $\text{nmol } \mu\text{g}^{-1}$  for panels a, b, and c, respectively) exceed the bounds of the colorbars. Maximum values for DMS**  
 6 **and DMS flux occur in the waters south of the Alaska Peninsula, whereas maximum DMS:chl-*a* occurs mid PSAE.**

7